High Accuracy Calculations of the eEDM Enhancement Factor W_d in YbCu, YbAg & YbAu

J. D. Polet

July 7, 2022

University of Groningen | Faculty Of Science & Engineering | Bachelor Thesis

Abstract

The electron electric dipole moment (eEDM) enhancement factor W_d and the scalar-pseudoscalar (S-PS) interaction enhancement factor W_S are required to determine the eEDM and S-PS interaction parameters from an experiment measuring an energy shift. In this thesis, these enhancement factors, along with the equilibrium bond distances, are determined for the YbCu, YbAg and YbAu molecules, to investigate whether these molecules are suitable to be utilized for eEDM searches. The computations are performed using the Fock space coupled cluster method. A triple zeta basis set is used for the computations of the W_d values for YbCu and YbAg, and all the W_S values, while a quadruple zeta basis set is used for the computation of W_d for YbAu. Relativity is treated with the four component Dirac Hamiltonian. The core orbitals of the molecules are frozen to reduce computational costs. The uncertainty of W_d is determined by performing many computations to identify the individual sources of error. One computation of W_S is performed to gauge its magnitude. The relative uncertainty found for W_d is attributed to W_S and a full uncertainty analysis should be done in further research. The found values are: $W_d = 12.98 \pm 1.27 \cdot 10^{24} \frac{\text{h Hz}}{\text{e cm}}$ for YbCu, $W_d = 11.76 \pm 0.98 \cdot 10^{24} \frac{\text{h Hz}}{\text{e cm}}$ for YbAg and $W_d = 1.31 \pm 0.33 \cdot 10^{24} \frac{\text{h Hz}}{\text{e cm}}$ for YbAu. The W_d to W_S ratio is found to be significantly lower for YbAu than for the other two molecules.

First Examiner - prof. dr. Anastasia Borschevsky
Second Examiner - prof. dr. Steven Hoekstra
Daily Supervisor - Yuly A. Chamorro Mena

university of groningen

Contents

Page

1. Introduction 4

2. Theory 6

2.1. Hamiltonian of the eEDM . . . 6

2.2. Hamiltonian of the S-PS interaction . . . 6

2.3. Perturbation on the relativistic Dirac-Coulomb Hamiltonian . . . 6

2.4. Ratio and other parameters . . . 7

3. Computational considerations 8

3.1. Born-Oppenheimer approximation . . . 8

3.2. Molecular orbital theory . . . 8

3.3. Relativistic Hamiltonians . . . 8

3.4. Electron correlation . . . 10

3.5. Basis sets . . . 10

3.6. Methods . . . 12

3.6.1. Dirac-Hartree-Fock . . . 12

3.6.2. Coupled cluster . . . 14

3.6.3. Fock space coupled cluster . . . 16

3.6.4. Møller–Plesset perturbation theory . . . 18

3.7. Vibrational correction . . . 19

3.8. Further considerations . . . 20

3.8.1. Finite field approach . . . 20

3.8.2. Equilibrium bond length . . . 21

4. Results 22

4.1. Geometry optimization . . . 22

4.2. Field strength . . . 25

4.3. Electron correlation . . . 26

4.3.1. Active occupied space . . . 26

4.3.2. Virtual space cut-off . . . 28

4.4. Basis set . . . 30

4.5. Method and relativity . . . 31

4.6. Geometry 32
4.6.1. Vibrational correction 33
4.7. Uncertainty 34
4.8. Final Values 38

5. Discussion 39

6. Conclusion 41

7. Acknowledgements 42

8. Bibliography 43

Appendix A. Additional results 47
A.1. Equilibrium bond length 47
A.2. Field strength 47
A.3. Electron correlation 49

1. Introduction

In recent years, there have been many phenomena discovered that cannot be explained by the Standard Model of particle physics. These phenomena include, but are not limited to, neutrino oscillations, the matter-antimatter asymmetry in the universe and the existence of dark matter and dark energy [1–3]. In an effort to explain these phenomena, many new theories have emerged, often referred to as beyond the Standard Model (BSM) theories, or new-physics theories. Some examples of these new theories are: the supersymmetry models, where every Standard Model particle acquires a supersymmetric partner particle, or extradimensional theories, that introduce extra dimensions on top of the four-dimensional spacetime that is currently assumed [4].

To solve some of the main questions within particle physics, it will be essential to determine which of the many new-physics theories yields the most accurate description of reality. A useful probe to test these theories is the electric dipole moment of the electron (eEDM) [5]. The existence of an eEDM violates both parity ($\mathcal{P}$) and time reversal ($\mathcal{T}$) conservation. This is because under parity transformation, the eEDM switches sign while the spin of the electron does not and under time reversal the opposite occurs [6]. Then, if we assume that total $\mathcal{CPT}$ symmetry is conserved, $\mathcal{T}$ violation implies the combined $\mathcal{CP}$ violation (where $\mathcal{C}$ denotes the charge conjugation) [1].

According to the Standard Model, the eEDM arises from the $\mathcal{CP}$ violating components of the CKM matrix[1]. The effect is caused by electrons coupling to virtual particles and is thus expected to be very small [1]. The Standard Model predicts an eEDM of $|d_e| < 10^{-38}$ e cm [8], which is not measurable with the current practical limitations [5]. Many of the new-physics theories predict the eEDM to be orders of magnitude larger (mostly between $10^{-25} - 10^{-33}$ e cm [9]). This increase of the predicted value of the eEDM is caused by a higher degree of $\mathcal{CP}$ violation, which is required to explain the matter-antimatter asymmetry in the universe [1].

To actually measure the eEDM, high precision experiments are required. Still, this value cannot be measured directly. This is because an electric field is imperative for the measurement and since the electron is charged, the electric field will accelerate the electron away from the experiment[2] [10]. To find the value of the eEDM, either atoms or molecules are required, since the eEDM can interact with the internal electric fields within these particles, which results in an energy shift that can be measured [11]. The outer shell of these systems will be an open shell, since for closed-shell systems, there is no energy shift to be measured. The internal electric field from the point of view of the valence electron is the effective electric field E_{eff} [12]. The E_{eff} is directly proportional to the W_d parameter that will be found in this research. The energy shift in the particles will be tiny, so system with a large enhancement factor W_d have to be used [13].

The energy shift that is measured in these experiments is not only due to the eEDM. The second interaction that contributes to the found energy shift is the scalar-pseudoscalar (S-PS) interaction, which has its own enhancement factor W_S and interaction parameter k_s [5]. These are analogous to W_d and d_e for the eEDM interaction. To determine the eEDM, not only W_d needs to be known, but W_S has to be known as well. Furthermore, to decouple the k_s and d_e interaction parameters, measurements on two different systems are required, as will become clear in Section 2.4.

The eEDM enhancement factor W_d is required to be as large as possible. There are multiple key characteristics of systems that give rise to a large W_d. First, molecules are preferred over atoms since they possess more degrees of freedom — both rotational and vibrational — and therefore, more and denser energy levels. Then, since the energy differences between the levels are smaller,

[1] The CKM or Cabibbo-Kobayashi-Maskawa matrix describes the mixing between the mass eigenstates and flavour eigenstates of quarks [7].

[2] A proposal for the direct measurement of the eEDM has been made, which uses magnetic storage rings and is further explained in [10].

the effect of a perturbative coupling is amplified [14]. Also, since the eEDM enhancement factor is roughly proportional to the atomic number cubed, a molecule with at least one heavy atom will drastically increase W_d [11]. Furthermore, the molecule should be as polar as possible to increase W_d [14], which can be done by choosing atoms with unequal electronegativities [15].

The ACME collaboration found the current upper limit of the eEDM to be $|d_e| < 1.1 \cdot 10^{-29}$ e cm [16], using a molecular beam of thorium monoxide (ThO) which has many of the properties described above. Since this value is below some of the predictions from the BSM theories, those theories have either been discarded or have had to restrict their parameters [17].

The molecules discussed in this research (YbCu, YbAg and YbAu) contain at least one heavy atom[3] and are polar molecules, with the electronegativity of the coinage-metal atoms being at least 0.8 larger than that of ytterbium[4] according to the Pauling scale, which fixes the electronegativity of fluorine to 3.98 and that of caesium to 0.79 [19]. The chosen molecule should possess an unpaired electron spin in its ground state, which is the case for the molecules in question, since the ytterbium atom has a closed outer shell and the coinage-metals have an unpaired s-electron in the valance shell [13]. Then, since the sensitivity of the measurement increases linearly with the coherent interaction time, the molecules will have to be cooled and trapped to produce an accurate result [5]. Since the ytterbium-containing molecules consist of two metals, it is possible to assemble the molecule from ultracooled atoms instead of having to laser-cool the molecule itself, which is a difficult process [15].

So, the three ytterbium-containing molecules seem to be promising candidates to start looking for the eEDM in high precision experiments. The measured quantity during the experiment will be the energy shift, so to find the corresponding value of the electric dipole moment of the electron, the enhancement factor needs to be known among other parameters. This factor cannot be found through experiments and has to be calculated numerically [5]. This research will provide a value for the eEDM enhancement factor W_d for YbCu, YbAg and YbAu, with benchmark uncertainty, using ab initio[5] calculations. This is implemented by first looking into the theory behind the eEDM enhancement factor in Section 2. Subsequently, the main computational considerations to take into account for the calculations will be explained in Section 3. Then, in Section 4 the results of the calculations will be compared and the optimal combination of parameters will be used to acquire W_d with the lowest possible uncertainty. In Section 5 the accuracy of the results will be discussed and compared to previous works. Finally, in Section 6 a summary and recommendations will be given. For the rest of the thesis, Hartree atomic units ($\hbar = e = a_0 = m_e = 1$) will be implied unless stated otherwise explicitly.

[3]For YbCu and YbAg the heavier atom is ytterbium with atomic number 70 and for YbAu the heavier atom is gold with atomic number 79.

[4]The Pauling electronegativity of ytterbium is 1.1, of copper is 1.90, of silver is 1.93 and of gold is 2.54 [18].

[5]Ab initio means "from first principles" in Latin, and in this context, that the only inputs used for the calculations are physical constants.

2. Theory

In this section, the equation for the enhancement factor of the eEDM and the equation for the enhancement factor of the S-PS interaction will be derived by using first-order perturbation theory on the relativistic Dirac-Coulomb Hamiltonian.

2.1. Hamiltonian of the eEDM.

To find the value of the eEDM enhancement factor W_d, the effect of the eEDM on the system is required. The Hamiltonian for the interaction caused by the eEDM is given by

$$\hat{H}^{eEDM} = -d_e(\gamma^0 \boldsymbol{\Sigma} \cdot \boldsymbol{E} + i\boldsymbol{\gamma} \cdot \boldsymbol{B}), \tag{1}$$

where d_e is the eEDM, $\boldsymbol{E}$ the total electric field, $\boldsymbol{B}$ the total magnetic field, $\gamma^\mu = \{\gamma^0, \boldsymbol{\gamma}\} = \{\gamma^0, \gamma^1, \gamma^2, \gamma^3\}$ denotes the Dirac gamma matrices, which are

$$\gamma^0 = \begin{bmatrix} \mathbb{1}_{2\times2} & \emptyset_{2\times2} \\ \emptyset_{2\times2} & -\mathbb{1}_{2\times2} \end{bmatrix}, \quad \gamma^1 = \begin{bmatrix} 0 & 0 & 0 & 1 \\ 0 & 0 & 1 & 0 \\ 0 & -1 & 0 & 0 \\ -1 & 0 & 0 & 0 \end{bmatrix}, \quad \gamma^2 = \begin{bmatrix} 0 & 0 & 0 & -i \\ 0 & 0 & i & 0 \\ 0 & i & 0 & 0 \\ -i & 0 & 0 & 0 \end{bmatrix}, \quad \gamma^3 = \begin{bmatrix} 0 & 0 & 1 & 0 \\ 0 & 0 & 0 & -1 \\ -1 & 0 & 0 & 0 \\ 0 & 1 & 0 & 0 \end{bmatrix}$$

and $\boldsymbol{\Sigma}$ denotes the vector of Pauli spin matrices, given by

$$\boldsymbol{\Sigma} = \begin{bmatrix} \boldsymbol{\sigma} & \emptyset_{2\times2} \\ \emptyset_{2\times2} & \boldsymbol{\sigma} \end{bmatrix}, \qquad \sigma_x = \begin{bmatrix} 0 & 1 \\ 1 & 0 \end{bmatrix}, \qquad \sigma_y = \begin{bmatrix} 0 & -i \\ i & 0 \end{bmatrix}, \qquad \sigma_z = \begin{bmatrix} 1 & 0 \\ 0 & -1 \end{bmatrix}.$$

The second term of the Hamiltonian, describing the interaction of the eEDM with the magnetic field, is negligible when compared to the term describing the interaction of the eEDM with the electric field [5]. Then, the effective eEDM Hamiltonian can be described by a one-body operator, given by

$$\hat{H}_{\mathit{eff}}^{eEDM} = 2icd_e \sum_i^n \gamma^5 \beta \boldsymbol{p}_i^2, \tag{2}$$

where n is the total number of electrons of the system, c is the speed of light in vacuum, β is one of the Dirac matrices defined in Equation 7, $\boldsymbol{p}_i$ is the momentum of electron i and $\gamma^5 = i\gamma^0\gamma^1\gamma^2\gamma^3$ [20, 21]. A full derivation from Equation 1 to Equation 2 can be found in [22].

2.2. Hamiltonian of the S-PS interaction.

Just as for the eEDM enhancement factor, W_S will also follow from an expectation value of a Hamiltonian. Now, the Hamiltonian describing the S-PS interaction is required, which is defined as

$$\hat{H}^{S\text{-}PS} = i\frac{G_F}{\sqrt{2}} Z k_s \sum_i^n \gamma^0\gamma^5 \rho(\boldsymbol{r}_i), \tag{3}$$

where again the Dirac gamma matrices appear, along with the Fermi constant G_F, the atomic number Z, the dimensionless electron-nucleus S-PS coupling constant k_s and the nuclear charge density $\rho(\boldsymbol{r}_{iN})$ [23]. The Fermi constant is $2.2225 \cdot 10^{-14}$ in atomic units [5] and the dimensionless constant k_s can be split up, giving $Zk_s = Zk_{s,p} + Nk_{s,n}$, where $k_{s,p}$ is the eletron-proton coupling constant, $k_{s,n}$ is the eletron-neutron coupling constant and N is the neutron number [23].

2.3. Perturbation on the relativistic Dirac-Coulomb Hamiltonian.

Now, the Hamiltonian caused by the eEDM can be used as a first-order perturbation to a model Hamiltonian to obtain the total electronic Hamiltonian,

$$\hat{H}_{el} = \hat{H}^{(0)} + \lambda \frac{\hat{H}^{eEDM}}{d_e} = \hat{H}^{(0)} + \lambda 2ic \sum_i^n \gamma^5 \beta \boldsymbol{p}_i^2. \tag{4}$$

Similarly, the S-PS Hamiltonian is treated as a perturbation,

$$\hat{H}_{el} = \hat{H}^{(0)} + \lambda \frac{\hat{H}^{S\text{-}PS}}{k_s} = \hat{H}^{(0)} + \lambda i \frac{G_F}{\sqrt{2}} Z \sum_i^n \gamma^0 \gamma^5 \rho(\boldsymbol{r}_i). \tag{5}$$

Here, λ is the field strength which is chosen such that λ^2-terms and higher order terms can be ignored. For the purposes of this research, the field strength will be equal for both interactions, although different values could be taken. Then, $\hat{H}^{(0)}$ is the relativistic Dirac-Coulomb Hamiltonian, given by

$$\hat{H}^{(0)} = \sum_i^n \left[\beta_i mc^2 + c\boldsymbol{\alpha}_i \cdot \hat{\boldsymbol{p}}_i - V_{NN}(r_i) \right] + \frac{1}{2} \sum_{i \neq j}^n \frac{1}{r_{ij}}, \tag{6}$$

where m is the electron mass, V_{NN} is the Coulomb potential due to the nucleus, r_i is the distance between electron i and the nucleus, r_{ij} is the distance between electrons i and j and the Dirac matrices $\boldsymbol{\alpha}$ and β are given by

$$\boldsymbol{\alpha} = \begin{bmatrix} \emptyset_{2\times2} & \boldsymbol{\sigma} \\ \boldsymbol{\sigma} & \emptyset_{2\times2} \end{bmatrix}, \qquad \beta = \begin{bmatrix} \mathbb{1}_{2\times2} & \emptyset_{2\times2} \\ \emptyset_{2\times2} & -\mathbb{1}_{2\times2} \end{bmatrix}. \tag{7}$$

The Dirac-Coulomb Hamiltonian is based on the Born-Oppenheimer approximation, which will be further explained in Section 3.1. Then, since perturbation theory is employed, the expectation value of the Hamiltonian in Equation 4 can be expanded in a Taylor series around $\lambda = 0$,

$$E_\Omega = E_\Omega^{(0)} + \lambda E_\Omega^{(1)} + \lambda^2 E_\Omega^{(2)} + \mathcal{O}(\lambda^n). \tag{8}$$

Now, because of the choice of λ, the terms with λ^2 and all higher order terms will vanish, leaving

$$E_\Omega = E_\Omega^{(0)} + \lambda E_\Omega^{(1)}. \tag{9}$$

Thus, the eEDM enhancement factor is given by

$$W_d = \frac{1}{\Omega} \frac{dE_\Omega}{d\lambda}\bigg|_{\lambda=0} = \frac{E_{eff}}{\Omega} \approx \frac{\left\langle \hat{H}_{eff}^{eEDM} \right\rangle}{\Omega}, \tag{10}$$

where Ω is the electronic angular momentum projected along the internuclear axis [5, 12, 13]. It is equal to $\frac{1}{2}$ for the $X^2\Sigma^+$ ground states of the YbCu, YbAg and YbAu molecules [24]. Similarly, the S-PS interaction enhancement factor is given by

$$W_S = \frac{1}{\Omega} \frac{dE_\Omega}{d\lambda}\bigg|_{\lambda=0}, \tag{11}$$

where the value will be different from W_d, due to the different perturbation used in the process [5].

2.4. **Ratio and other parameters.** As mentioned in the introduction, to determine d_e, both W_d and W_S are required. This is because the electric dipole moment that is measured during experiments can be expressed as,

$$d_{para} \approx W_d \cdot d_e + W_S \cdot k_s. \tag{12}$$

From Equation 12, it can be observed that at least two measurements of the electric dipole moments of systems with a different $\frac{W_S}{W_d}$ ratio are required to disentangle the values of d_e and k_s. The other parameters that can influence the value of d_{para} are orders of magnitude smaller than the contributions from the eEDM and the S-PS interaction for diatomic molecules [25].

3. **Computational considerations**

In theory, solving the full Schrödinger or Dirac equation will yield the exact energy of a system. However, the sad and harsh truth of the matter is that fully modelling a system such as a molecule takes too much computational effort. This indicates that some approximations need to be made, which will reduce the accuracy of the calculation, but will decrease the computational costs. Furthermore, there are a variety of methods that can be employed to find the energy of a system. These approximations, methods and other considerations will be explained in the rest of this section.

3.1. **Born-Oppenheimer approximation.**

The approximation that is fundamental for many computational methods to reduce the computational complexity of the calculation, is the Born-Oppenheimer (BO) approximation or adiabatic approximation. This approximation assumes that the nuclei of a system stay in a fixed position, while the electrons move around the nuclei. This approximation is really efficient and only slightly affects the calculated chemical properties of the system [26]. The approximation works so well, since the nuclei of a system are typically far heavier than the surrounding electrons, therefore their relative velocity will be way lower.

Using the BO approximation, the total wavefunction of a system can be separated into a nuclear part and an electronic part. Then, the full Hamiltonian can also be split up into an electronic Hamiltonian and a nuclear Hamiltonian [27]. The general form of the electronic Hamiltonian will be given by

$$\hat{H}_{el} = \sum_{i}^{n} \hat{h}(i) + \frac{1}{2} \sum_{i \neq j}^{n} \hat{g}(i,j) + V_{NN}, \tag{13}$$

where n is the total number of electrons within the system, $\hat{h}(i)$ is the one-electron operator, $\hat{g}(i,j)$ is the two-electron operator and V_{NN} is the potential between the nuclei [28].

3.2. **Molecular orbital theory.**

For atoms, electrons are described by orbital wavefunctions, but it is not completely clear what happens to these orbitals when atoms are placed together into molecules [29]. One approach to approximate the molecular orbitals (MOs) is to assume that they consist of a linear combination of atomic orbitals (AOs),

$$\chi = \sum_{A}^{N} C_A \phi_A, \tag{14}$$

where χ is the MO, ϕ_A is the AO of atom A, N is the number of atoms within the molecule and C_A is a linear coefficient. This is the LCAO-MO approximation, and it is used by the computational methods that study molecules [26].

3.3. **Relativistic Hamiltonians.**

Including relativity will be important for the calculation of the eEDM and S-PS enhancement factors. This is because the electrons surrounding the heavy nuclei of the molecules can reach velocities close to the velocity of light. It has been found that both the W_d parameter and the W_S parameter increase for increasing atomic number Z. The actual dependence differs for each group in the periodic table of elements, although a general approximation for W_d is given by

$$W_d \approx -\frac{4}{3} \frac{Z^3 \alpha^2 \varkappa}{\gamma^4}, \tag{15}$$

where $\alpha \approx \frac{1}{137}$ is the fine structure constant, $\varkappa$ is a constant that depends on the effective electronic structure of the system and $\gamma = \frac{1}{\sqrt{1-\frac{v^2}{c^2}}}$ is the Lorentz factor with velocity v and speed of light c.

The approximation for the S-PS enhancement factor is given by

$$W_S \approx -\frac{G_F}{2\pi\sqrt{2}a_0^3} R(Z,A)\gamma Z^3 \alpha \varkappa, \tag{16}$$

where a_0 is the Bohr radius and $R(Z,A)$ is a relativistic enhancement factor. Although both approximations contain different constants, their dependence on the atomic number is equal. The true power of Z can vary between $\sim 2.5-3.8$ depending on the system [21]. Consequently, relativity is an important contribution to the W_d and W_S factors for molecules containing heavy atoms.

As a matter of fact, when going to the non-relativistic limit, there will not be a measurable energy shift and therefore, no eEDM can be determined, due to Schiff's theorem [1, 11]. This follows from the fact that, a non-relativistic particle experiencing the sum of an internal electric field from other particles and an external electric field, has a Hamiltonian

$$H = \frac{p^2}{2m} + q\phi, \tag{17}$$

where $\boldsymbol{p}$ is the particle's momentum, m is its mass, q is its charge and ϕ is the total electrostatic potential. Then, since the total electric field $\boldsymbol{E}_{tot} = -\boldsymbol{\nabla}\phi$ and the momentum $\boldsymbol{p} = -i\hbar\boldsymbol{\nabla}$, the expectation value of $\boldsymbol{E}_{tot}$ will vanish for any eigenstate. Thus, the energy shift $\langle \hat{H}^{eEDM} \rangle = -\boldsymbol{d}_e \cdot \langle \boldsymbol{E}_{tot} \rangle = 0$. As a result, to evade Schiff's theorem, relativity has to be included to ensure a measurable energy shift [1].

The choice of Hamiltonian is usually defined by the amount of components that are used for the one electron operator (as defined in Equation 13). In the non-relativistic regime, the one electron operator is a scalar, hence it is described by one component (1c). When relativity is added to the system, this gives rise to the existence of the antiparticle of the electron, the positron [30]. Now, the one electron operator has four components (4c), describing both the particle and the antiparticle with their spins. It is also possible to use two component (2c) Hamiltonians, where the positronic part of the 4c Hamiltonian has been frozen. The spin-orbit interaction, caused by the interaction of the electron spin with the magnetic field created by the motion of the electron [31], is already described well by the 2c Hamiltonian. However, full relativity is best described by the 4c Hamiltonian [28]. Another useful Hamiltonian is the spin-free (SF) Hamiltonian, which removes the spin orbit interaction from the 4c Hamiltonian.

Generally, the 2c Hamiltonian will be less accurate in calculating the properties of particles, since it is missing the degrees of freedom from the antiparticle. Yet, a new Hamiltonian has been developed, which is the exact two component (X2c) Hamiltonian. This Hamiltonian is able to match the results of the 4c Hamiltonian for the positive energy solutions. Usually, this method is less computationally heavy than the 4c Hamiltonian [28].

The overall best technique to describe the relativity of the system would be to use full quantum electrodynamics (QED). However, solving the QED Hamiltonian is not feasible for many-particle systems. So instead, we resort to the Dirac Hamiltonian with the Born Oppenheimer approximation. The difficulty for this Hamiltonian lies within the two-electron operator $\hat{g}(i,j)$. This operator can be expanded as a Taylor series in $\frac{1}{c}$ and the terms up to $\frac{1}{c^2}$ then yield,

$$\hat{g}(i,j) = \hat{g}^{Coulomb}(i,j) + \hat{g}^{Breit}(i,j), \tag{18}$$

$$= \hat{g}^{Coulomb}(i,j) + \hat{g}^{Gaunt}(i,j) + \hat{g}^{Gauge}(i,j), \tag{19}$$

$$= \frac{\mathbb{1}_{4\times4}}{r_{ij}} - \frac{\boldsymbol{\alpha}_i \cdot \boldsymbol{\alpha}_j}{r_{ij}} + \left[\frac{\boldsymbol{\alpha}_i \cdot \boldsymbol{\alpha}_j}{2r_{ij}} - \frac{\left(\boldsymbol{\alpha}_i \cdot r_{ij}\right)\left(\boldsymbol{\alpha}_j \cdot r_{ij}\right)}{2r_{ij}^3} \right], \tag{20}$$

where $\boldsymbol{\alpha}$ is the Dirac matrix as defined in Section 2.3, the Coulomb term is the zeroth-order approximation of the full Coulomb interaction and the Breit term is the first-order correction, consisting of the Gaunt interaction term and the Gauge interaction term [31, 32]. The Coulomb term describes the time-independent action between electrons, not taking relativity into account. The Breit term adds the delay to the Coulomb interaction caused by relativity [31]. The Gaunt term describes the spin-other-orbit, spin-spin and orbit-orbit interactions, while the Gauge term describes the spin-free or scalar interaction. Usually, the Gauge term is less important than the Gaunt term [32].

3.4. **Electron correlation.** While relativity is treated by the Hamiltonian, the electron correlation is determined by the method [32]. The methods will be explained in Section 3.6. The electron correlation describes the interaction between the electrons within the molecular orbitals. Coulomb correlation is the interaction between electrons with opposite spin, and Fermi correlation is the interaction between electrons with the same spin. The Coulomb correlation will be the largest contribution to the full correlation, since it occurs between electrons within the same orbital and between electrons within separate orbitals. The Fermi correlation cannot occur between electrons within the same orbital due to Pauli's exclusion principle.

The static electron correlation is given by electrons within the system seeing all the other electrons as a charge distribution, while the dynamic correlation will be given by the excitation of the electrons. In a system, the orbitals that contain electrons are the occupied orbitals, while the rest of the orbitals are virtual orbitals. If electrons get excited, they move to these virtual orbitals. Usually, the valence electrons are more likely to be excited, since the energy gap between the valence electrons and the first virtual orbital is minute. This implies that the core orbitals can be frozen to reduce computational costs [31]. The active space cut-off is generally set at -20 a.u.[6], however to get highly accurate results for properties such as the eEDM enhancement factor or the S-PS enhancement factor, this will not be enough. This is because W_d and W_S are very dependent on the correlation of core electrons. The usual cut-off for the virtual orbitals lies at 30 a.u.. Yet again, for this research, this virtual space cut-off should be extended significantly, since high-lying virtual orbitals are essential for capturing the electron correlation of the core electrons [5].

3.5. **Basis sets.** To describe the electrons of a molecule, the molecular orbitals have to be constructed, this is done by using one-particle basis functions. Together, these basis functions form a basis set [34]. There are a variety of ways to perform the construction of the orbitals. Since the LCAO-MO approximation (explained in Section 3.2) is utilized, the AOs will be constructed first, which will then form the MOs. The AOs are composed of a general form,

$$\phi_{nlm}(r,\theta,\phi) = R_n(r)Y_{lm}(\theta,\phi), \tag{21}$$

where $R_n(r)$ is the radial part and $Y_{lm}(\theta,\phi)$ the angular part of the AO wavefunction. The radial part can be described by either Slater type orbitals (STOs) or Gaussian type orbitals (GTOs). Then, in Cartesian coordinates they take the forms

$$\phi_{mno}^{STO} = Nx^m y^n z^o e^{-\zeta r}, \qquad \phi_{mno}^{GTO} = Nx^m y^n z^o e^{-\zeta r^2}. \tag{22}$$

Here, m, n and o define the total angular momentum as $L = m + n + o$, $\dfrac{1}{\zeta}$ defines the width of the orbital, $r = \sqrt{x^2 + y^2 + z^2}$ and N is a normalization factor [35].

The actual behaviour of the orbitals is better described by the STO, it has a cusp at the origin and the right exponential decay, but it is computationally heavy. The cusp near the origin is necessary, due to the nuclear cusp condition. This condition states that when the electron is coinciding with the nucleus, the electronic Hamiltonian has to become singular [36]. The GTO functions can be evaluated more rapidly, although the behaviour near the core and the outer regions is not correct,

[6] 1 a.u. or one Hartree is equal to 27.211 386 245 988 eV [33].

as can be seen from Figure 1. This can be solved by using a linear combination of GTOs to mimic the behaviour of the STO. This requires less computational cost than the STO itself, therefore using a linear combination of GTOs is the preferred method to use [34]. Now, the GTO is described as a contracted Gaussian type orbital (CGTO) consisting of primitive Gaussian type orbitals (PGTOs),

$$\phi^{CGTO} = \sum_{j=1}^{K} c_j \phi_j^{PGTO}, \qquad \phi_j^{PGTO} = \sum_{i=1}^{M} d_{ij} \chi_i. \tag{23}$$

Here, K is the number of used PGTOs per CGTO, M is the number of Gaussians used per PGTO, d_{ij} are fixed linear coefficients and χ_i are fixed basis functions [37].

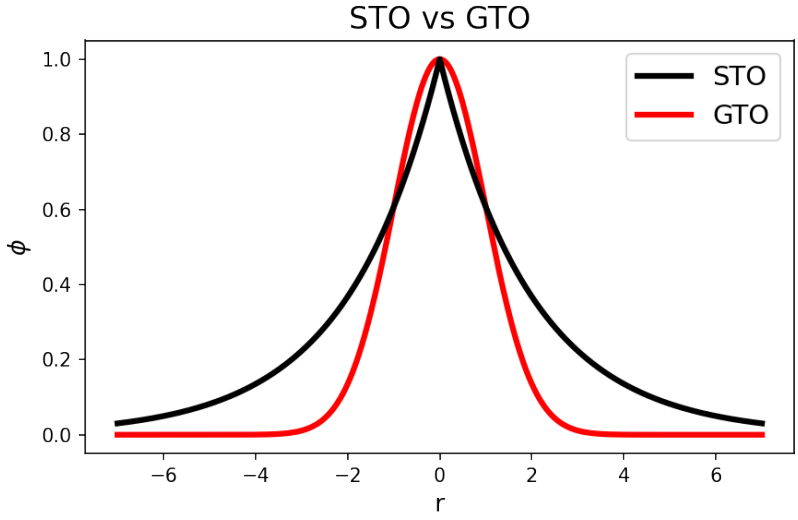

FIGURE 1. An example plot showing the differences between a Slater type orbital and a Gaussian type orbital.

When a single basis function (either an STO, GTO or CGTO) is used for each AO, this is called the minimal basis set or single zeta (Sz) basis set. Using two independent basis functions per AO is a double zeta (Dz) basis. This can proceed to triple zeta (Tz), quadruple zeta (Qz) and further [34, 37]. The number of basis functions used per orbital gives the cardinality of the basis set. Using a larger basis set, i.e. using more basis functions per AO, increases both the accuracy and the computational cost of the calculation. When an infinite number of basis functions is used per AO, the basis set is complete and the resulting energy is the complete basis set (CBS) limit. This CBS value can be derived by extrapolating the found values for smaller basis sets [38]. For the computations in this work, Dyall's uncontracted relativistic basis sets were employed [39].

Split valence basis sets (vXz) use just a single basis function for the core electrons[7] and multiple basis functions for the valence electrons. In the case of vQz, four basis functions are used per AO in the valence region.

These basis sets can be improved by adding either tight or diffuse basis functions to the orbitals. Tight functions will have a small width, hence they can increase the quality of the description of the AO near the nucleus and the core electrons. If tight functions are added to the basis set, it is then usually indicated as cvXz, a core-valence basis set with X functions per orbital in the core region and the valence region. Diffuse functions will have a large width, therefore they can increase the quality of the description of the AO in the outer regions of the system, near the valence electrons

[7]The core electrons are those with a lower principal quantum number than the valence electrons.

[34]. If diffuse functions are added to the basis set, it is then usually indicated as s-aug-vXz, a single diffuse function is augmented to a basis set with X functions per orbital [5].

3.6. **Methods.** To obtain the molecular properties of a system, one needs to solve the time-independent electronic Schrödinger equation to obtain the energy, or the Dirac equation when dealing with a 4c Hamiltonian. There are many various computational methods that approach this problem from a variety of angles. In this subsection, the Dirac-Hartree-Fock approach, the coupled cluster method, the Fock space coupled cluster method and the Møller–Plesset perturbation theory will be discussed in detail, since these approaches will be used in Section 4 to obtain the eEDM enhancement factor.

3.6.1. **Dirac-Hartree-Fock.** The Dirac-Hartree-Fock (DHF) approach is one of the simpler methods to solve the time-independent electronic Schrödinger equation. It is a variational method that is based on the assumption that every electron within the system sees all the other electrons as a charge distribution with which it can interact. Thus, it is referred to as a mean field theory. For the derivation of this method, the notes by David Sherrill provided in [40] will be followed. This method does not include electron correlation as described in Section 3.4. The difference between the true energy and the energy found using the DHF method is called the correlation energy. The time-independent electronic Schrödinger equation is given by

(24)
$$\hat{H}_{el}^{NR}\left|\Psi(\boldsymbol{r};\boldsymbol{R})\right\rangle = \left(-\frac{1}{2}\sum_{i}^{n}\nabla_i^2 - \sum_{A,i}^{N,n}\frac{Z_A}{r_{Ai}} + \sum_{A>B}^{N}\frac{Z_A Z_B}{R_{AB}} + \sum_{i>j}^{n}\frac{1}{r_{ij}}\right)\left|\Psi(\boldsymbol{r};\boldsymbol{R})\right\rangle = E_{el}\left|\Psi(\boldsymbol{r};\boldsymbol{R})\right\rangle,$$

where $\hat{H}_{el}^{NR}$ is the non-relativistic electronic Hamiltonian, Ψ the electronic wavefunction, $\boldsymbol{r}$ the electronic coordinates, $\boldsymbol{R}$ the nuclear coordinates, N the total amount of nuclei, Z_X the atomic number of nucleus X, R_{AB} the distance between nuclei A and B and E_{el} the electronic energy. This cumbersome long expression for the Hamiltonian can be simplified by expressing it in terms of one-electron operators and two-electron operators, using a variation of Equation 13,

$$\hat{H}_{el}^{NR} = \sum_{i}^{n}\hat{h}(i) + \sum_{i<j}^{n}\hat{v}(i,j) + V_{NN}, \tag{25}$$

where now,

$$\hat{h}(i) = -\frac{1}{2}\nabla_i^2 - \sum_{A}^{N}\frac{Z_A}{r_{iA}}, \qquad \hat{v}(i,j) = \frac{1}{r_{ij}}$$

and V_{NN} is the Coulomb potential between the nuclei described by $\sum_{A>B}^{N}\frac{Z_A Z_B}{R_{AB}}$ in Equation 24. Here, the two-electron operator does not include the Breit correction, as defined in Section 3.3, to simplify the calculations.

The DHF method's first guess for the electronic wavefunction is the Hartree product,

$$\Psi_{HP} = \chi_1(\boldsymbol{x}_1)\chi_2(\boldsymbol{x}_2)\cdots\chi_n(\boldsymbol{x}_n), \tag{26}$$

where $\chi_i(\boldsymbol{x}_i)$ is the spin-orbital of electron i, which is the product of the spatial orbital and a spin function (α or β[8]). This wavefunction does not satisfy Pauli's principle, since it is not antisymmetric under exchange of any two electrons. This can be solved by using a specific linear combination of

[8]Generally, α is the spin up wavefunction and β is the spin down wavefunction.

these spin-orbitals which is given by the Slater determinant [26, 40]

$$\Psi = \frac{1}{\sqrt{n!}} \begin{vmatrix} \chi_1(\boldsymbol{x}_1) & \chi_2(\boldsymbol{x}_1) & \cdots & \chi_n(\boldsymbol{x}_1) \\ \chi_1(\boldsymbol{x}_2) & \chi_2(\boldsymbol{x}_2) & \cdots & \chi_n(\boldsymbol{x}_2) \\ \vdots & \vdots & \ddots & \vdots \\ \chi_1(\boldsymbol{x}_n) & \chi_2(\boldsymbol{x}_n) & \cdots & \chi_n(\boldsymbol{x}_n) \end{vmatrix} \equiv |12\cdots n\rangle \,. \tag{27}$$

Now, each row contains the orbitals and each column the electrons. This wavefunction is indeed antisymmetric, since the determinant switches sign under exchange of either rows or columns. Also, the wavefunction vanishes if there are two electrons in the same quantum state, since the determinant vanishes when two rows or columns are equal [41].

Then, by using the variational theorem with the Hamiltonian from Equation 25 and the Slater determinant as the wavefunction, the Hartree-Fock energy can be derived to be

$$E_{HF} = \sum_{i}^{n} \langle i|\hat{h}|i\rangle + \frac{1}{2}\sum_{ij} \left[(ii|jj) - (ij|ji)\right], \tag{28}$$

where $\langle i|\hat{h}|j\rangle$ is a one electron integral denoted by

$$\langle i|\hat{h}|j\rangle = \int \chi_i^*(\boldsymbol{x}_1)\hat{h}(i)\chi_j(\boldsymbol{x}_1)\, d\boldsymbol{x}_1 \tag{29}$$

and $(ij|kl)$ is a two-electron integral denoted by

$$(ij|kl) = \int \chi_i^*(\boldsymbol{x}_1)\chi_j(\boldsymbol{x}_1)\frac{1}{r_{ij}}\chi_k^*(\boldsymbol{x}_2)\chi_l(\boldsymbol{x}_2)\, d\boldsymbol{x}_1 d\boldsymbol{x}_2. \tag{30}$$

Since the DHF approach is a variational method, the Hartree-Fock energy will always be an upper limit to the true energy of the system.

To optimize the wavefunction given by a single Slater determinant, the Hartree-Fock energy needs to be minimized by varying the orbitals. The constraint for the variation is that the orbitals should stay orthonormal throughout the entire variational procedure, therefore the constraint equation is $\langle i|j\rangle = \delta_{ij}$. Then, by using the Lagrange method of undetermined multipliers and finding the minimum of the Lagrangian, the Hartree-Fock equations can be derived,

$$\left\{\hat{h}(\boldsymbol{x}_1) + \sum_{j\neq i}^{n}\left[\mathcal{J}_j(\boldsymbol{x}_1) - \mathcal{K}_j(\boldsymbol{x}_1)\right]\right\}\chi_i(\boldsymbol{x}_1) = \epsilon_i\chi_i(\boldsymbol{x}_1). \tag{31}$$

Here, ϵ_i is the energy eigenvalue associated with the spin-orbital $\chi_i(\boldsymbol{x}_1)$, $\mathcal{J}_j(\boldsymbol{x}_1)$ is the Coulomb term which gives the potential at $\boldsymbol{x}_1$ from the average charge distribution of the electron in orbital $\chi_j(\boldsymbol{x}_2)$ and is denoted by

$$\mathcal{J}_j(\boldsymbol{x}_1) = \int \frac{|\chi_j(\boldsymbol{x}_2)|^2}{r_{12}}\, d\boldsymbol{x}_2 \tag{32}$$

and $\mathcal{K}_j(\boldsymbol{x}_1)$ is the exchange operator which exchanges the orbitals and is a requirement to satisfy the antisymmetry of the wavefunction. It is denoted by

$$\mathcal{K}_j(\boldsymbol{x}_1)\chi_i(\boldsymbol{x}_1) = \left[\int \frac{\chi_j^*(\boldsymbol{x}_2)\chi_i(\boldsymbol{x}_2)}{r_{12}}\, d\boldsymbol{x}_2\right]\chi_j(\boldsymbol{x}_1). \tag{33}$$

The Hartree-Fock equations can be further simplified by introducing the Fock operator,

$$\hat{f}(\boldsymbol{x}_1) = \hat{h}(\boldsymbol{x}_1) + \sum_{j}^{n}\left[\mathcal{J}_j(\boldsymbol{x}_1) - \mathcal{K}_j(\boldsymbol{x}_1)\right]. \tag{34}$$

Then, the nonlinear Hartree-Fock equations are given by

$$\hat{f}(\boldsymbol{x}_1)\chi_i(\boldsymbol{x}_1) = \epsilon_i\chi_i(\boldsymbol{x}_1). \tag{35}$$

The solutions to these equations can be found by guessing an initial trial orbital wavefunction, calculating the Fock operator and then solving Equation 35 to obtain new orbital wavefunctions. Next, these new orbitals are used for the calculations, and this process continues until convergence. This is where the energy of the new orbitals is within a threshold value of the energy of the previous orbitals [26]. Thus, solving the Hartree-Fock equations is an iterative procedure and hence, the DHF method is a self-consistent-field (SCF) approach [40]. The iteration is required, since the Fock operator is dependent on the orbitals.

The DHF method illustrated in this section only allows for orbitals that are occupied by two electrons, therefore it is known as the restricted Hartree Fock (RHS) method. If one allows for the two spin orbitals to have different spatial orbitals, a pair of coupled equations is found, one for spin up and one for spin down [42]. This method is known as the spin-unrestricted Hartree Fock method (UHF). Both methods can be used for open-shell and closed-shell systems [26].

Both RHS and UHF have the property that they are size-extensive. This means, that the energy calculated using these methods scales linearly with the number of electrons in the system. The methods differ in size-consistency, which is the property that if two systems are far apart, they should not be able to interact with each other, and that the behaviour of the total energy should be correctly described for all separations. Generally, both methods are size-consistent. However, for excitations into open-shell systems UHF is size-consistent, whereas RHF is not size-consistent [43].

3.6.2. **Coupled cluster.** Another method to solve the time-independent electronic Schrödinger equation is the coupled cluster (CC) method. This method is perturbative, so it does not yield an upper limit to the energy of the system. However, it is one of the most effective methods to use. Although, that does mean that this method is computationally expensive. It can be used for the calculation of properties of molecules in the ground state and low excited states [44]. Unlike the DHF method, the CC method does include electron correlation, hence it will be more accurate. To introduce this method, the derivation by Ira N. Levine given in [45] will be followed. The CC method is based on the definition of the cluster operator $\hat{T}$ and the fundamental equation is given by

$$\Psi = e^{\hat{T}}\Phi_0, \tag{36}$$

where Ψ is the exact wavefunction and Φ_0 is some model wavefunction, for instance a Slater determinant. The exponential of the cluster operator can be expanded as a Taylor series,

$$e^{\hat{T}} \equiv 1 + \hat{T} + \frac{\hat{T}^2}{2!} + \frac{\hat{T}^3}{3!} + \cdots. \tag{37}$$

The Taylor expansion is performed, since only a couple of these terms will actually be used in this method to save resources. The cluster operator, or excitation operator, can be split up in the following way,

$$\hat{T} = \hat{T}_1 + \hat{T}_2 + \cdots + \hat{T}_n. \tag{38}$$

Here, $\hat{T}_1$ is the one-particle excitation operator, $\hat{T}_2$ is the two-particle excitation operator and $\hat{T}_n$ is the n-particle excitation operator, where n again is the number of electrons within the system. The one- and two-particle excitation operators are defined as,

$$\hat{T}_1\Phi_0 = \sum_{a=n+1}^{\infty}\sum_{i=1}^{n} t_i^a\Phi_i^a, \qquad \hat{T}_2\Phi_0 = \sum_{b=n+1}^{\infty}\sum_{a=n+1}^{\infty}\sum_{j=i+1}^{n}\sum_{i=1}^{n-1} t_{ij}^{ab}\Phi_{ij}^{ab}, \tag{39}$$

where the indices $i, j, \cdots$ indicate occupied orbitals and $a, b, \cdots$ indicate virtual orbitals. The one-particle excitation operator excites an electron from orbital i to orbital a as described by the singly excited Slater determinant Φ_i^a. The amplitude of this excitation is given by the numerical coefficient t_i^a. Similarly, the two-particle excitation operator excites two electrons from orbitals i and j to orbitals a and b as described by the doubly excited Slater determinant Φ_{ij}^{ab}. The amplitude of this excitation is given by the numerical coefficient t_{ij}^{ab}.

Next, the expression for the cluster operator will be truncated to reduce the computational costs. If only the one- and two-particle excitation operators are used, this gives the CC singles and doubles (CCSD) method. If the three-particle excitation operators are also included, this is the CCSDT method. For CCSD, Equation 37 becomes

$$e^{\hat{T}} = e^{\hat{T}_1+\hat{T}_2} = 1 + \hat{T}_1 + \hat{T}_2 + \frac{(\hat{T}_1+\hat{T}_2)^2}{2!} + \cdots = 1 + \hat{T}_1 + \hat{T}_2 + \frac{\hat{T}_1^2 + \hat{T}_2^2 + \hat{T}_1\hat{T}_2 + \hat{T}_2\hat{T}_1}{2!} + \cdots . \tag{40}$$

The term $\frac{1}{2!}\hat{T}_1^2$ describes a double excitation, with a product of two single-excitation amplitudes $t_i^a t_j^b$, which are disconnected contributions. This can be seen as two electrons being excited independently. This is similar to the $\hat{T}_2$ term, which also excites two electrons, however, the amplitude is now a single double-excitation amplitude t_{ij}^{ab}, which is a connected term. The term $\frac{1}{2!}\hat{T}_2^2$ describes a quadruple excitation, with a product of two double-excitation amplitudes $t_{ij}^{ab} t_{kl}^{cd}$, which are disconnected contributions. This can be seen as two electron pairs being excited independently. The other two terms ($\frac{1}{2!}\hat{T}_1\hat{T}_2$ and $\frac{1}{2!}\hat{T}_2\hat{T}_1$) describe the situation where three electrons are excited, one lone electron and one electron pair.

Then, the Schrödinger equation can be solved by using the wavefunction given in Equation 36,

$$\hat{H}\left|\Psi\right\rangle = E\left|\Psi\right\rangle \qquad \Longrightarrow \qquad \hat{H}\left|e^{\hat{T}}\Phi_0\right\rangle = E\left|e^{\hat{T}}\Phi_0\right\rangle. \tag{41}$$

Now, multiplying by the complex conjugate of the model wavefunction yields

$$\left\langle \Phi_0\middle|\hat{H}\middle|e^{\hat{T}}\Phi_0\right\rangle = E\left\langle \Phi_0\middle|e^{\hat{T}}\Phi_0\right\rangle = E\left(\langle\Phi_0|\Phi_0\rangle + \left\langle \Phi_0\middle|\hat{T}\Phi_0\right\rangle + \left\langle \Phi_0\middle|\frac{\hat{T}^2}{2!}\Phi_0\right\rangle + \cdots\right) = E. \tag{42}$$

This final equality is true, since $\langle\Phi_0|\Phi_0\rangle = 1$ and all the higher order terms vanish because all the spin-orbitals are orthogonal to each other and the higher order terms all contain an excited Slater determinant. Then, multiplying Equation 41 by $\left\langle \Phi_{ij}^{ab}\right|$ and substituting Equation 42 gives the general CC equation,

$$\left\langle \Phi_{ij}^{ab}\middle|\,\hat{H}\,\middle|e^{\hat{T}}\Phi_0\right\rangle = E\left\langle \Phi_{ij}^{ab}\middle|e^{\hat{T}}\Phi_0\right\rangle = \left\langle \Phi_0\middle|\hat{H}\middle|e^{\hat{T}}\Phi_0\right\rangle\left\langle \Phi_{ij}^{ab}\middle|e^{\hat{T}}\Phi_0\right\rangle. \tag{43}$$

For CCSD, this becomes

$$\left\langle \Phi_{ij}^{ab}\middle|\,\hat{H}\,\middle|e^{\hat{T}_1}e^{\hat{T}_2}\Phi_0\right\rangle = \left\langle \Phi_0\middle|\hat{H}\middle|e^{\hat{T}_1}e^{\hat{T}_2}\Phi_0\right\rangle\left\langle \Phi_{ij}^{ab}\middle|e^{\hat{T}_1}e^{\hat{T}_2}\Phi_0\right\rangle. \tag{44}$$

The left-hand side of Equation 44 can be reduced to

$$\left\langle \Phi_{ij}^{ab}\middle|\hat{H}\middle|\left(1+\hat{\mathcal{T}}_5\right)\Phi_0\right\rangle, \tag{45}$$

where

$$\hat{\mathcal{T}}_5 = \hat{T}_1 + \hat{T}_2 + \frac{\hat{T}_1^2 + \hat{T}_2^2 + \hat{T}_1\hat{T}_2 + \hat{T}_2\hat{T}_1}{2!} + \frac{\hat{T}_1^3 + \hat{T}_2^2\hat{T}_1 + \hat{T}_1\hat{T}_2\hat{T}_1 + \hat{T}_2\hat{T}_1^2 + \hat{T}_1^2\hat{T}_2 + \hat{T}_1\hat{T}_2^2 + \hat{T}_2\hat{T}_1\hat{T}_2}{3!} + \frac{\hat{T}_1^4 + \hat{T}_1\hat{T}_2\hat{T}_1^2 + \hat{T}_2\hat{T}_1^3 + \hat{T}_1^2\hat{T}_2\hat{T}_1 + \hat{T}_1^3\hat{T}_2}{4!} + \frac{\hat{T}_1^5}{5!}. \tag{46}$$

All higher order terms vanish, since the Cordon-Slater rules show that matrix elements of the Hamiltonian between Slater determinants differing by four or more spin-orbitals vanish. Similarly, for the first integral on the right-hand side of Equation 44,

$$E_{CCSD} = \left\langle \Phi_0 \middle| \hat{H} \middle| e^{\hat{T}_1} e^{\hat{T}_2} \Phi_0 \right\rangle = \left\langle \Phi_0 \middle| \hat{H} \middle| \left(1 + \hat{T}_1 + \hat{T}_2 + \frac{\hat{T}_1^2 + \hat{T}_1\hat{T}_2 + \hat{T}_2\hat{T}_1}{2!} + \frac{\hat{T}_1^3}{3!} \right) \Phi_0 \right\rangle, \tag{47}$$

$$= E_{HF} + \left\langle \Phi_0 \middle| \hat{H} \middle| \left(\hat{T}_1 + \hat{T}_2 + \frac{\hat{T}_1^2 + \hat{T}_1\hat{T}_2 + \hat{T}_2\hat{T}_1}{2!} + \frac{\hat{T}_1^3}{3!} \right) \Phi_0 \right\rangle, \tag{48}$$

$$\equiv E_{HF} + \left\langle \Phi_0 \middle| \hat{H} \middle| \hat{\mathcal{T}}_3 \Phi_0 \right\rangle, \tag{49}$$

where E_{HF} is the Hartree-Fock energy and $\hat{\mathcal{T}}_3$ denotes the sum of one-, two- and three-electron excitations. As for the final integral in Equation 44, it is only non-zero if $e^{\hat{T}_1} e^{\hat{T}_2}$ excites two electrons due to the orthogonality of the Slater determinants. Therefore, it reduces down to

$$\left\langle \Phi_{ij}^{ab} \middle| e^{\hat{T}_1} e^{\hat{T}_2} \Phi_0 \right\rangle = \left\langle \Phi_{ij}^{ab} \middle| \left(\hat{T}_1^2 + \hat{T}_2 \right) \Phi_0 \right\rangle. \tag{50}$$

Subsequently, Equation 44 can be written like

$$\left\langle \Phi_{ij}^{ab} \middle| \hat{H} \middle| \left(1 + \hat{\mathcal{T}}_5 \right) \Phi_0 \right\rangle = \left(E_{HF} + \left\langle \Phi_0 \middle| \hat{H} \middle| \hat{\mathcal{T}}_3 \Phi_0 \right\rangle \right) \left\langle \Phi_{ij}^{ab} \middle| \left(\hat{T}_1^2 + \hat{T}_2 \right) \Phi_0 \right\rangle. \tag{51}$$

Then, this equation can be further rewritten in terms of amplitudes. This becomes a number of equations with an equal number of unknowns (amplitudes) which can be solved iteratively to obtain the amplitudes. Finally, using the amplitudes, the CCSD energy can be found. A similar derivation can be performed for CCSDT and higher order methods.

The CCSDT method requires significantly more computation time than the CCSD method, since it scales as N^8, compared to N^6 for CCSD, where N is the size of the basis set [28]. To find a middle ground, the fourth-order terms of CCSDT can be added to CCSD to create the CCSD + T method [46]. The method that is used most frequently, adds a subset of fifth-order terms along with the fourth-order terms to CCSD, creating the CCSD(T) method. This method scales as N^7 and is thus less computationally heavy than the full CCSDT method [47, 48]. The final CC method that will be used, is the CCSD − T method, which adds another fifth-order perturbation term to CCSD(T) [46].

All CC methods are size-extensive. Furthermore, CC methods are also size-consistent, provided that an RHF determinant is not used as the model determinant. If RHF is used as a foundation for the CC method, systems exciting to open-shell states will not be size-consistent [49].

Currently, it is too computationally demanding to include QED effects and the Breit correction to the molecular CC method. However, adding QED effects and the Gaunt and Gauge interaction terms would improve the accuracy of the final result.

3.6.3. **Fock space coupled cluster.** The single-reference CC (SRCC) method introduced in the previous section works especially well for closed-shell systems, but performs worse for open-shell systems. This is mainly due to the use of a single Slater determinant as the model wavefunction [50]. Since all three molecules considered in this work contain an electron in an open shell, optimizing the CC method would produce more accurate results.

To improve upon the SRCC method, the single Slater determinant can be changed to a manifold of reference states (model space). This model space then forms the basis of the multi-reference CC (MRCC) method. There are two main types of MRCC approaches: the Hilbert-space MRCC

(HSCC) and the Fock-space MRCC (FSCC) [51]. The method described here is the FSCC, which requires calculations of the system for states with a different number of electrons [52]. The FSCC method starts with a closed-shell system and then either adds or removes electrons until the desired state is reached [53].

In the FSCC method, the orbitals (configuration space) are split up into three parts: the core orbitals, which are occupied, the valence orbitals, from which electrons can get excited, and the virtual orbitals, which are unoccupied. The model space P represents the valence orbitals, while the orthogonal space Q represents the core orbitals and virtual orbitals. The model space is d-dimensional and spanned by the model determinants, thus its projection operator can be described by

$$\hat{P}_M^{(p,h)} = \sum_i^d |\Phi_i\rangle \langle\Phi_i| , \tag{52}$$

where p stands for particles, h stands for holes, Φ_i is the model determinant i, and d is the amount of model determinants used. If d is more than one, then the method is a multi-reference method. The projection operator of the orthogonal space, or complementary space can be described by

$$\hat{Q}_M^{(p,h)} = 1 - \hat{P}_M^{(p,h)}. \tag{53}$$

The model and orthogonal spaces can be split up into sectors, the four main sectors are defined here. $\hat{P}_M^{(0,0)}$ generates the model space that consists of just a single determinant Φ_0, while then the orthogonal space $\hat{Q}_M^{(0,0)}$, consists of all the excited determinants. $\hat{P}_M^{(0,1)}$ generates the model space for singly ionized states[9], since there is a hole in the model space. $\hat{P}_M^{(1,0)}$ generates the model space for the wavefunction with one attached electron. $\hat{P}_M^{(1,1)}$ generates the model space for states where a single electron is excited from a core orbital to a virtual orbital [51].

Now, these projection operators will be used to determine the correlation energy using the effective Hamiltonian formalism. Starting with the Schrödinger equations

$$\hat{H} |\Psi_i\rangle = E_i |\Psi_i\rangle , \qquad i = 1, \cdots, m, \tag{54}$$

with exact eigenfunctions Ψ_i. The earlier defined projection operator for the model space can project the exact eigenfunctions onto the model space, giving the projected eigenfunctions

$$\left|\tilde{\Psi}_i\right\rangle = \hat{P}_M^{(p,h)} |\Psi_i\rangle . \tag{55}$$

Then, a new operator $\hat{\Omega}$, the universal wave operator, is introduced that performs the opposite projection as $\hat{P}_M^{(p,h)}$, defined as

$$|\Psi_i\rangle = \hat{\Omega} \left|\tilde{\Psi}_i\right\rangle , \qquad \hat{\Omega} =: e^{\tilde{S}^{(p,h)}} :, \tag{56}$$

where the colons that surround the exponential indicate that the operator within the colons is normal ordered, such that all annihilation operators are placed to the right [30, 54]. The term in the exponential of Equation 56 is the cluster operator or excitation operator of FSCC, defined by

$$\tilde{S}^{(p,h)} = \sum_{k=0}^{p} \sum_{l=0}^{h} \hat{S}^{(k,l)}, \tag{57}$$

where the cluster operator of a particular sector can be described as [50, 55]

$$\hat{S}^{(k,l)} = \hat{S}_1^{(k,l)} + \hat{S}_2^{(k,l)} + \cdots + \hat{S}_n^{(k,l)}. \tag{58}$$

[9] In other works, the sectors are also sometimes indicated by (h,p) instead of (p,h).

Equation 58 can be truncated to reduce the computational costs. If only the single and double excitations are taken into account, this is the FSCCSD method. This method will be used for the computations in this work.

To solve the set of equations, the Bloch equation is used. The normal ordering done in Equation 56 ensures that the equations are decoupled. Then, the specific Bloch equations only contain operators of its own sector and lower sectors [55].

The Schrödinger equation from Equation 54 can be rewritten in terms of projected eigenfunctions, yielding

$$\hat{H}\hat{\Omega}\left|\tilde{\Psi}_i\right\rangle = E_i\hat{\Omega}\left|\tilde{\Psi}_i\right\rangle. \tag{59}$$

Then, by bringing the universal wave operator to the left side of Equation 59, the effective Hamiltonian can be defined as

$$\hat{H}_{\mathit{eff}}\left|\tilde{\Psi}_i\right\rangle = \hat{\Omega}^{-1}\hat{H}\hat{\Omega}\left|\tilde{\Psi}_i\right\rangle = E_i\left|\tilde{\Psi}_i\right\rangle. \tag{60}$$

Next, by imposing the intermediate normalization $\hat{P}\hat{\Omega}\hat{P} = \hat{P}$, the effective Hamiltonian can be described by

$$\hat{H}_{\mathit{eff}} = \hat{P}\hat{H}\hat{\Omega}\hat{P} = \hat{H}_0 + \hat{V}_{\mathit{eff}}. \tag{61}$$

Finally, the dynamic correlation can be determined from

$$\hat{Q}(\hat{H}\hat{\Omega} - \hat{\Omega}\hat{H}_{\mathit{eff}})\hat{P} = 0, \tag{62}$$

which follows from projecting Equation 59 on the orthogonal space Q [54].

An alternative derivation of the FSCC approach can be found in [56].

3.6.4. **Møller–Plesset perturbation theory.** The final method that will be used in this research is the Møller–Plesset (MP) perturbation theory, which builds on the DHF method explained in Section 3.6.1. It does this by adding the missing electron correlation as a perturbation to DHF. Following the derivations by Christopher Cramer in [57] and Ira Levine in [45], MP sets the model Hamiltonian to the sum of the one-electron Fock operators,

$$\hat{H}^{(0)} = \sum_i^m \hat{f}_i, \tag{63}$$

where m is the number of basis functions. The zeroth-order energy is given by the eigenvalue equation,

$$\hat{H}^{(0)}\Phi_0 = E^{(0)}\Phi_0 = \sum_i^n \epsilon_i\Phi_0, \tag{64}$$

where Φ_0 is the Slater determinant as defined in Section 3.6.1. The electron correlation is added by using the correction term

$$V = \sum_i^n \left\{ \sum_{j>i}^n \frac{1}{r_{ij}} - \sum_j^n \left[\mathcal{J}_j(\boldsymbol{x}_1) - \mathcal{K}_j(\boldsymbol{x}_1)\right] \right\}. \tag{65}$$

Now, the first-order correction yields the Hartree-Fock energy,

$$E_{MP1} = E^{(0)} + E^{(1)}, \tag{66}$$

$$= \langle\Phi_0|\hat{H}^{(0)}|\Phi_0\rangle + \langle\Phi_0|V|\Phi_0\rangle\,, \tag{67}$$

$$= \langle\Phi_0|\hat{H}^{(0)} + V|\Phi_0\rangle\,, \tag{68}$$

$$= \langle\Phi_0|\hat{H}|\Phi_0\rangle\,, \tag{69}$$

$$= E_{HF}. \tag{70}$$

So far, no electron correlation has been added. This will be implemented from the second-order correction onwards. This second-order correction is given by

$$E^{(2)} = \sum_{i=j+1}^{n}\sum_{j=1}^{n-1}\sum_{a=n+1}^{\infty}\sum_{b=a+1}^{\infty}\frac{\big[(ij|ab) - (ia|jb)\big]^2}{\epsilon_i + \epsilon_j - \epsilon_a - \epsilon_b}, \tag{71}$$

where again, like for the CC approach, the indices $i, j, \cdots$ indicate occupied orbitals and the indices $a, b, \cdots$ indicate virtual orbitals. Then, for MP2[10], $E_{MP2} = E^{(0)} + E^{(1)} + E^{(2)}$.

MP2 calculations are quite rapid and scale with N^5. The MP2 method will not always lead to the best results, as perturbations are supposed to be small, while the electron correlation effects can become relatively large. Only once the fourth-order corrections are taken into account (MP4), does the result become more accurate, however, MP4 already scales as N^7, so it becomes computationally heavy. Furthermore, convergence is not typically observed when increasing the order of perturbation theory for MP, making it a less desirable method to use than, for instance, CC.

Similar to CC methods, MP methods are always size-extensive, and they are size-consistent as long as it is based on a UHF method [49].

3.7. **Vibrational correction.** In this research, the calculations will be performed by assuming that the distance between the two atoms of the molecule is equal to the equilibrium bond length[11]. However, as mentioned in the introduction, molecules possess (among other degrees of freedom) vibrational degrees of freedom. This is represented by vibrational energy levels in the potential energy diagram shown in Figure 2. The value of these energy levels is given by

$$E_\nu = \left(\nu + \frac{1}{2}\right)\omega, \qquad \omega = \sqrt{\frac{k_f}{m_{eff}}}, \qquad m_{eff} \approx \frac{m_1 m_2}{m_1 + m_2}, \tag{72}$$

where ν is the vibrational quantum number, k_f represents the stiffness of the bond between the atoms and m_i is the mass of atom i [58].

Now, the lowest vibrational energy level is not zero and therefore this level does not intersect the electronic potential energy curve at the equilibrium bond length. This implies that in the ground state, the molecules still include some freedom to vibrate, oscillating back and forth between the two intersections with the electronic potential energy curve. The electronic potential energy curve is not symmetric, but has an anharmonic component, as can be seen from Figure 2. So, the value of the W_d factor at the equilibrium bond length will be slightly different from the average value in the lowest vibrational energy level. This difference is the vibrational correction. In the figure, this is the difference between the equilibrium bond length R_e and the effective equilibrium bond length R_e^{eff}.

[10]MP2 is also occasionally mentioned as MBPT(2), denoting the general many-body perturbation theory [45].

[11]The terms equilibrium bond length, equilibrium bond distance and geometry are used interchangeably throughout this thesis.

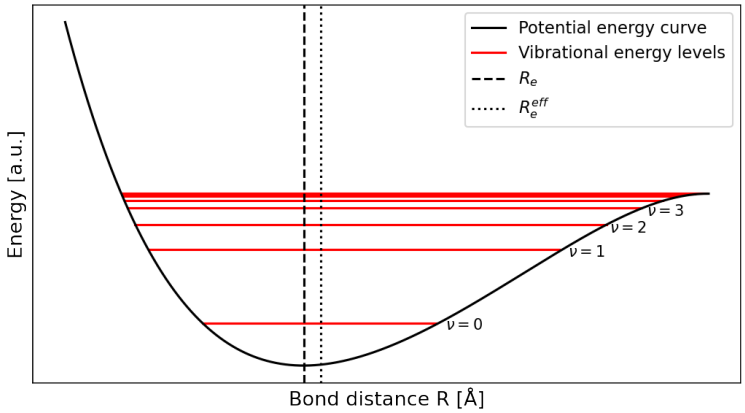

FIGURE 2. The general molecular potential energy curve with vibrational levels. The minimum of the potential curve determines the equilibrium bond length R_e. The average bond length in the lowest vibrational level determines the effective equilibrium bond length R_e^{eff}.

3.8. **Further considerations.** Apart from all the considerations taken into account so far, there are two more points to be considered. Particularly, the finite field approach and the equilibrium bond distance. The finite field approach yields a method to extract W_d from multiple energy calculations and will be further explained in Section 3.8.1. The equilibrium bond distance is the distance between the nuclei of a molecule. The geometry has to be given as an input value for the computations. This parameter will be discussed in Section 3.8.2.

3.8.1. **Finite field approach.** Generally, the result of a calculation will be a total energy. Since the total energy is not the value that is searched for in this work, but rather the W_d and W_S properties, the finite field approximation is used. Using Equation 10 and Equation 11, combined with the fact that the field strength λ has to be small, the eEDM enhancement factor can be approximated as

$$W_d = \frac{1}{\Omega} E_{eff} = \frac{1}{\Omega} \left. \frac{dE_\Omega}{d\lambda} \right|_{\lambda=0} \approx \frac{1}{\Omega} \frac{E(\lambda) - E(-\lambda)}{2\lambda} \tag{73}$$

and similarly, the S-PS interaction enhancement factor can be approximated as

$$W_S = \frac{1}{\Omega} \left. \frac{dE_\Omega}{d\lambda} \right|_{\lambda=0} \approx \frac{1}{\Omega} \frac{E(\lambda) - E(-\lambda)}{2\lambda} \tag{74}$$

These definitions of W_d and W_S ensure that if there is a contribution from the λ^2 term, it will cancel out, since $\lambda^2 = (-\lambda)^2$. Any higher order terms will be negligible. Thus, the energy curve is expected to be linear in the regime of the field strength.

The quality of this linear fit can be checked by comparing the total energies from the positive and negative perturbations with the total energy without perturbation ($\lambda = 0$). To quantify the linearity of the fit, the R^2 value can be utilized. If this value is equal to one, that indicates that the linear fit is a perfect fit for the given data points. A fit resembling a horizontal line at the average of all the data points would yield $R^2 = 0$ and worse fits give negative R^2 values. The equation that determines R^2 is

$$R^2 = 1 - \frac{\sum_{i=1}^{m} (X_i - Y_i)^2}{\sum_{i=1}^{m} \left(\overline{Y} - Y_i\right)^2}, \tag{75}$$

where m is the amount of data points, X_i is the value predicted by the fit, Y_i is the actual value of data point i and $\overline{Y}$ is the average of the true values [59].

In this work, the found energies are in atomic units, but the unit of E_{eff} is $\mathrm{GV\,cm^{-1}}$, the unit of W_d is $\frac{\mathrm{h\ Hz}}{\mathrm{e\ cm}}$ and the unit of W_S is h kHz. The conversion between units is done in the following way. First, for the effective electric field, 1 a.u. $= 5.142\,206\,747\,63 \cdot 10^{11}\,\mathrm{V\,m^{-1}}$ [60]. Then,

$$E_{eff}\,[\mathrm{GV\,cm^{-1}}] = 5.14220674763 \cdot \frac{E(\lambda) - E(-\lambda)}{2\lambda}. \tag{76}$$

Next, for W_d the value of Planck's constant is used, which is $h = 4.135\,667\,696 \cdot 10^{-15}\,\mathrm{Hz\,eV^{-1}}$ [61]. Furthermore, to increase readability, a factor 10^{24} is generally taken into the unit, giving

$$W_d\left[10^{24}\,\frac{\mathrm{h\ Hz}}{\mathrm{e\ cm}}\right] = \frac{5.14220674763}{4.135667696}\frac{1}{\Omega}\frac{E(\lambda) - E(-\lambda)}{2\lambda} = 1.24338006 \cdot \frac{1}{\Omega}\frac{E(\lambda) - E(-\lambda)}{2\lambda}. \tag{77}$$

Finally, for W_S, some constants given in Equation 3 are not yet taken into account in the computation, so they have to be added along with the conversion to the right units. Furthermore, the atomic number given in that equation will be the atomic number of ytterbium, since the valence electron of the system belongs mostly to that atom. Using $h = 6.626\,070\,15 \cdot 10^{-34}\,\mathrm{J\,Hz^{-1}}$ [62], 1 a.u. $= 4.359\,744\,722\,207\,1 \cdot 10^{-18}\,\mathrm{J}$ [63], $Z_{Yb} = 70$ and $G_F = 2.2225 \cdot 10^{-14}$ a.u., the conversion becomes,

$$W_S[\mathrm{h\ kHz}] = \frac{4.3597447222071 \cdot 10^{-18}}{6.62607015 \cdot 10^{-34}} \cdot 2.2225 \cdot 10^{-14} \cdot 70 \cdot \frac{1}{1000} \cdot \frac{1}{\Omega}\frac{E(\lambda) - E(-\lambda)}{2\lambda}, \tag{78}$$

$$= 10.23634326 \cdot \frac{1}{\Omega}\frac{E(\lambda) - E(-\lambda)}{2\lambda}. \tag{79}$$

3.8.2. **Equilibrium bond length.** To compute the W_d and W_S factors, the geometry of the molecules in question needs to be known. The equilibrium bond distance will be used as an input for the calculations. The values of these distances for YbCu, YbAg and YbAu were found in [24] and are given by

$$R_e^{YbCu} = 2.910\,\text{Å}, \qquad R_e^{YbAg} = 3.063\,\text{Å}, \qquad R_e^{YbAu} = 2.939\,\text{Å}. \tag{80}$$

These values were obtained by using the CCSD(T) method, a quintuple zeta basis set and a non-relativistic Hamiltonian. Scalar relativistic effects were added afterwards by replacing the inner-shell electrons with pseudopotentials [24]. This relativistic treatment is not sufficient for determining the eEDM and S-PS enhancement factors, so the geometry will be optimized in Section 4.1.

4. **Results**

All the results presented within this section were obtained using the DIRAC19 program on the peregrine computer cluster located at the University of Groningen [64]. Most of this section will be devoted to investigate how the value of the eEDM enhancement factor W_d changes when using different computational methods. These results will be used to accurately determine the uncertainty of the final found W_d values. Only a single calculation will be done for the S-PS interaction enhancement factor W_S to gauge its magnitude and compute the W_d to W_S ratio. A full uncertainty analysis of W_S is out of the scope of this thesis.

4.1. **Geometry optimization.**

For all the calculations that will be performed throughout the rest of this section, the equilibrium bond lengths of YbCu, YbAg and YbAu are required.

The equilibrium bond distances were already given in Section 3.8.2, but only scalar relativistic effects were incorporated into those calculations. This means that the values can be optimized to include explicit relativistic effects.

The values of the equilibrium bond length for the three ytterbium-containing molecules given by Tomza in [24] did not include the spin-orbit relativistic effects, while for the rest of the calculations these will be taken into account. Furthermore, the quintuple zeta basis set that was used is not feasible for the computation of the W_d parameter, as this will be too computationally expensive.

So, the geometry (equilibrium bond distance) was optimized through the DIRAC program. To see what the effect of using different basis sets is, the optimization was performed using a v2z, a v3z and a v4z basis set, where a single diffuse function was augmented to the v4z basis set. Furthermore, the effect of using a relativistic Hamiltonian was tested by performing calculations using a 1c Hamiltonian, a spin-free (SF) Hamiltonian and an X2c Hamiltonian. The spin-free Hamiltonian removes the spin-orbit interaction from the 4c Hamiltonian. Moreover, a calculation was done using the CCSD(T) method to observe the change compared to the CCSD result. All the found geometries are listed in Table 1.

TABLE 1. The dependence of the optimal geometry of YbCu, YbAg and YbAu on the basis set, the Hamiltonian and the method.

Method	Basis set	Hamiltonian	YbCu R_e [Å]	YbAg R_e [Å]	YbAu R_e [Å]
CCSD	v2z	X2c	2.7401	2.8989	2.7088
CCSD	v3z	X2c	2.7747	2.8821	2.7086
CCSD	s-aug-v4z	X2c	2.7543	2.8589	2.6524
CCSD	v3z	1c	2.8612	3.0508	3.0576
CCSD	v3z	SF	2.7801	2.8822	2.7158
CCSD	v3z	X2c	2.7747	2.8821	2.7086
CCSD	v2z	SF	2.7457	2.9044	2.7250
CCSD(T)	v2z	SF	2.6834	2.8697	-[1]

[1] The CCSD(T) computation of YbAu is not feasible with the current computational limitations.

Table 1 shows that when increasing the cardinality of the basis set, this generally decreases R_e. Thus, the computations with a smaller basis set are overestimated. Going from the SF Hamiltonian to the X2c Hamiltonian only changes R_e slightly. However, when going to the 1c Hamiltonian, completely different behaviour is observed. All the R_e values are significantly higher than with a relativistic Hamiltonian, and R_e now increases with increasing atomic number. Finally, adding some

triple excitations to the CC method reduces R_e, thus the CCSD method results are overestimated. Even though the three systems are open-shell systems, the CCSD results are still deemed accurate. The triple excitations added in the CCSD(T) method can be altered significantly by the system not being closed-shell. Therefore, the CCSD(T) method is not used for the determination of the optimal geometry.

All the results listed in Table 1, apart from the computations with the s-aug-v4z basis set, were computed using a built-in optimization program. This program computes the energy at an initial bond length and then uses algorithms to search for the geometry with a lower energy. This is done until convergence is reached. For the s-aug-v4z basis set, using this program was not feasible with the computational limits of DIRAC. So instead, multiple single-point energy calculations were performed at various bond lengths. Then, a fourth-order polynomial curve was fit through the data points to obtain a potential energy curve. This curve for the YbCu molecule can be seen in Figure 3 and the plots for the other two molecules can be found in Appendix A.1. In these plots, the minimum of the polynomial fit gives the equilibrium bond distance.

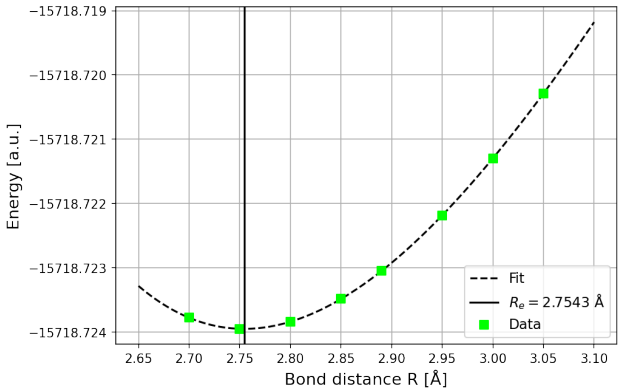

FIGURE 3. The potential energy curve of YbCu. The fit shown is a fourth-order polynomial. The minimum of this fit was chosen as the equilibrium bond distance R_e. The single-point energy calculations were performed using the CCSD method, an X2c Hamiltonian and the s-aug-v4z basis set. For the computations, 38 core electrons were frozen and the virtual space cut-off was set to 20 a.u..

TABLE 2. The optimized geometry computed using the built-in optimize program and derived from the potential energy curve (PEC), calculated using DIRAC for the v3z basis set, CCSD method and X2c Hamiltonian. 38, 46 and 64 core electrons were frozen for YbCu, YbAg and YbAu, respectively, and the virtual space cut-off was set to 20 a.u..

Molecule	R_e [Å] from built-in program	R_e [Å] from PEC
YbCu	2.77471	2.77460 (-0.0040%)
YbAg	2.88210	2.88161 (-0.0170%)
YbAu	2.70855	2.70820 (-0.0129%)

To ensure that the results from fitting a function to single-point energy calculations are accurate, this method was also applied to computations using the v3z basis set, CCSD method and X2c Hamiltonian. The differences between using the built-in program and the potential energy curve can be observed in Table 2. Since the difference in the optimal geometry is minute, it is assumed that both methods give equally accurate results for the equilibrium bond distance.

The values for the geometry that will be used for the rest of the computations were calculated using the s-aug-v4z basis set, the X2c Hamiltonian and the CCSD method. Here, to speed up the calculations, only virtual orbitals up to 20 a.u. and occupied orbitals up to −20 a.u. were taken into account for YbCu. For the other two molecules, since they contain more electrons, the active space cut-off was set to −10 a.u. and the virtual space cut-off to 10 a.u. This freezes 38 core electrons of YbCu, 64 core electrons of YbAg and 82 core electrons of YbAu, leaving 61, 53 and 67 valence electrons, respectively. Freezing the core orbitals is valid, since the geometry of the molecule is mostly dependent on the correlation of the valence electrons [65]. This is also the reason for augmenting diffuse Gaussians to the v4z basis set, since it improves the description of the orbitals in the valence region.

TABLE 3. The geometry as given by Tomza, and the optimized geometry calculated in this thesis using DIRAC for the s-aug-v4z basis set, CCSD method and X2c Hamiltonian. 38, 64 and 82 core electrons were frozen for YbCu, YbAg and YbAu, respectively, and the virtual space cut-off was set to 20 a.u. for YbCu and 10 a.u. for YbAg and YbAu.

Molecule	R_e [Å] from [24]	Optimized R_e [Å]
YbCu	2.910	2.7543
YbAg	3.063	2.8589
YbAu	2.939	2.6524

In Table 3, the optimized geometries and the geometries given by Tomza can be found for the three ytterbium-containing molecules studied in this work. The observed difference between the values is significant for all three molecules. There are multiple differences in the method of computation that could explain why the values do not correspond. First, Tomza [24] uses a quintuple zeta basis set with augmented functions for the coinage metals and a [10s10p9d5f3g] basis set for ytterbium, while in this work the s-aug-v4z basis set is utilized for both atoms. Second, in this work the CCSD method is used, as opposed to the CCSD(T) method used by Tomza. Third, relativity is treated differently in both works. The results in this thesis were obtained by employing the X2c Hamiltonian, whilst Tomza incorporates scalar relativistic effect by applying pseudopotentials. These distinctions in computational approaches contribute to the discrepancy between the found optimal geometries. Finally, Tomza corrects for the basis set superposition error with the Boys-Bernardi counterpoise correction, which is not done in this work. However, this correction is only a minor contribution to the found value.

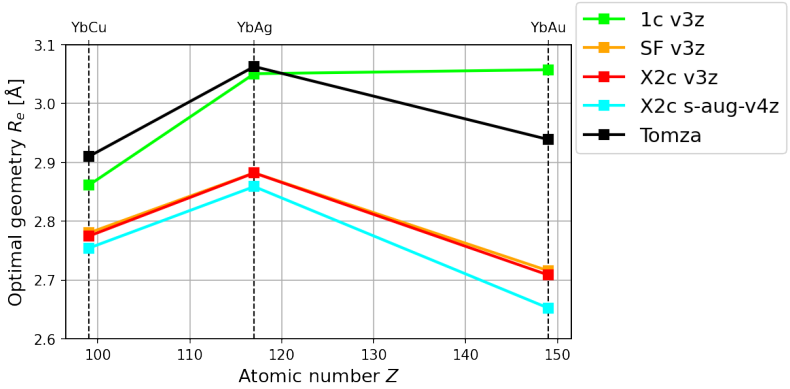

FIGURE 4. The optimal geometry against the atomic number of the diatomic molecules, computed using five different approaches.

In Figure 4, the results for the geometry optimization are plotted against the atomic numbers of the three diatomic molecules discussed in this thesis. Here, it can be observed that relativity becomes increasingly important for molecules with higher atomic numbers. For heavier molecules, the difference between using relativity or not increases. Furthermore, the general trend seems to be similar for both the X2c methods and Tomza's method, although the actual values are not alike.

Now the optimal geometry of the molecules has been determined, calculations on the W_d parameter can start. First, the optimal field strength will be determined for the molecules. Then, many of the computational considerations discussed in Section 3 will be varied to observe the effect on W_d.

4.2. **Field strength.** It is important to optimize the value of the field strength, since it should be small enough to suppress the higher order terms, but it should not be too small, as that will increase the final uncertainty in W_d. This can be observed by looking at Equation 73. Furthermore, if λ is smaller than the convergence threshold of the energy, the difference in positive and negative perturbations cannot be observed.

To find the optimal value to use for the field strength, molecular energy calculations were performed for various orders of magnitude of λ. For these calculations, the CCSD method was used with a v2z basis set. Relativity was included through an X2c Hamiltonian. Virtual orbitals up to 20 a.u. were taken into account and 38 core electrons were frozen for YbCu, 46 core electrons were frozen for YbAg and 64 core electrons were frozen for YbAu. The full results for the YbCu molecule can be seen in Figure 5. Similar graphs for YbAg and YbAu can be found in Appendix A.2.

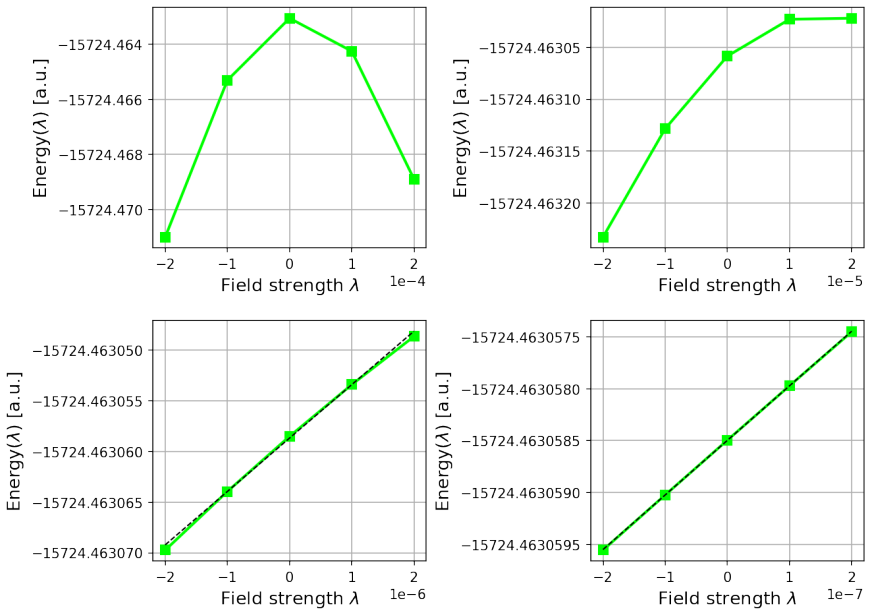

FIGURE 5. The dependence of the molecular energy of YbCu on the used field strength, using the optimized geometry, the v2z basis set, the CCSD method, a 4c Hamiltonian, a virtual space cut-off at 20 a.u. and freezing 38 core electrons. The dashed line shown in the bottom two plots represents a true linear relation.

The finite field strength approach detailed in Section 3.8.1 can only be employed if the positive and negative perturbations form a mostly linear relation. From the graphs displayed in Figure 5 it already becomes quite clear that for large field strength, there is little linearity, but to quantify this, the R^2 value was computed for each field strength. The R^2 values of the various field strengths of the three molecules can be found in Table 4.

TABLE 4. The R^2 value of a variety of field strength magnitudes for YbCu, YbAg and YbAu.

Field strength λ	YbCu R^2	YbAg R^2	YbAu R^2
$2 \cdot 10^{-4}$	0.0655292	0.0549037	0.0002440
$1 \cdot 10^{-4}$	0.2191710	0.1886607	0.0009507
$2 \cdot 10^{-5}$	0.8752893	0.8532536	0.0230588
$1 \cdot 10^{-5}$	0.9656056	0.9587768	0.0862482
$2 \cdot 10^{-6}$	0.9985775	0.9982834	0.7023336
$1 \cdot 10^{-6}$	0.9996438	0.9995705	0.9042136
$2 \cdot 10^{-7}$	0.9999859	0.9999829	0.9957781
$1 \cdot 10^{-7}$	0.9999965	0.9999957	0.9989474

From the figure, and by checking the goodness of the linear fits, it was decided to use a field strength of 10^{-6} for YbCu and YbAg, and a field strength of 10^{-7} for YbAu. These field strengths were chosen since they yield a highly linear relation between the positive and negative perturbation. Choosing a smaller field strength will only increase the error in W_d, which should be avoided.

4.3. **Electron correlation.** Now, using both the found geometry and field strength, the W_d parameter can be computed. In this section, the effect of electron correlation on W_d will be explored. This is done by first freezing various occupied orbitals and observing the difference compared to correlating all electrons. Second, the virtual space cut-off will be varied to see the effect of this parameter on W_d.

4.3.1. **Active occupied space.** Coupled cluster methods can correlate all electrons in the system. However, it is possible to freeze the core orbitals such that they are not taken into account for the electron correlation. The calculations in this section were performed using the FSCCSD method, a 4c Hamiltonian and a v2z basis set. The FSCCSD method is employed, since this method yields more accurate results for the open-shell systems than a regular CCSD approach. The virtual space cut-off for all of these computations was set to the same magnitude as the active space cut-off. So, if for a calculation the active space cut-off was set to -100 a.u., then the virtual space cut-off was set to 100 a.u..

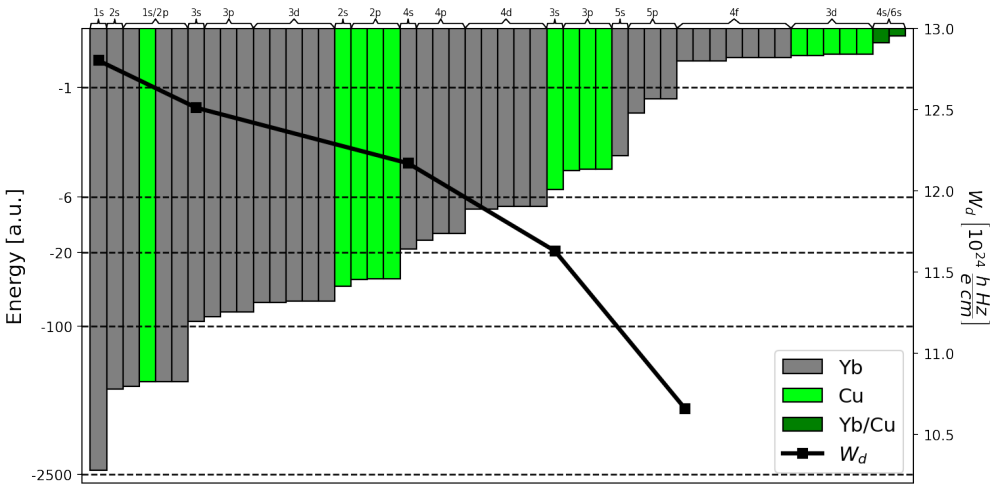

FIGURE 6. The energy of the molecular orbitals of YbCu. The used active space cut-offs are indicated with horizontal dashed lines. W_d is also plotted against the active orbitals.

The relation between the different used active space cut-offs and the number of correlated electrons for YbCu can be seen in Figure 6. Here, the molecular orbitals are split up into Cu orbitals and Yb orbitals, depending on the linear coefficient C_A, defined in equation 14. When $C_{Cu} \gg C_{Yb}$, the orbital is attributed to Cu, when $C_{Cu} \ll C_{Yb}$, the orbital is attributed to Yb and when both values are similar, the orbitals are split up between the two atoms. This is the case for the outer s-orbitals. The W_d values found when freezing some active orbitals is also displayed in the figure. Similar figures of YbAg and YbAu can be found in Appendix A.3.

In Table 5, the effect of electron correlation on W_d can be seen for YbCu. When freezing just over 12 percent of the total number of electrons, W_d already decreases by 2.27 percent. This shows that the core orbitals have a significant effect on the eEDM enhancement factor. When freezing even more orbitals, W_d reduces further.

TABLE 5. The eEDM enhancement factor of YbCu computed while freezing a different number of orbitals. The W_d values were computed using the FSCCSD method, a 4c Hamiltonian and a v2z basis set. N_{elec}^{corr} is the number of correlated electrons and N_{elec}^{total} is the total number of electrons in the system. The final column gives the relative difference of W_d compared to correlating all electrons.

Active(−)/virtual(+) space cut-off [a.u.]	N_{elec}^{corr}	$\frac{N_{elec}^{corr}}{N_{elec}^{total}}$	Frozen orbitals Yb	Cu	W_d $\left[10^{24}\frac{\text{h Hz}}{\text{e cm}}\right]$	Difference [%]
±1	27	0.2727	[Xe]	[Ar]	10.656	-16.77
±6	43	0.4343	[Kr]4d^{10}	[Ne]	11.629	-9.16
±20	61	0.6162	[Ar]3d^{10}	[Ne]	12.169	-4.95
±100	87	0.8788	[Ne]	[He]	12.512	-2.27
±2500	99	1	-	-	12.803	-

TABLE 6. The eEDM enhancement factor of YbAg computed while freezing a different number of orbitals. The W_d values were computed using the FSCCSD method, a 4c Hamiltonian and a v2z basis set. N_{elec}^{corr} is the number of correlated electrons and N_{elec}^{total} is the total number of electrons in the system. The final column gives the relative difference of W_d compared to correlating all electrons.

Active(−)/virtual(+) space cut-off [a.u.]	N_{elec}^{corr}	$\frac{N_{elec}^{corr}}{N_{elec}^{total}}$	Frozen orbitals Yb	Ag	W_d $\left[10^{24}\frac{\text{h Hz}}{\text{e cm}}\right]$	Difference [%]
±0.8	27	0.2308	[Xe]	[Kr]	9.153	-22.01
±10	53	0.4530	[Kr]	[Ar]3d^{10}	10.966	-6.57
±30	79	0.6752	[Ar]3d^{10}	[Ne]	11.268	-3.99
±100	97	0.8291	[Ne]	[Ne]	11.477	-2.21
±2500	117	1	-	-	11.737	-

Similarly, the results of freezing orbitals of YbAg and YbAu can be found in Table 6 and Table 7, respectively. Again, for YbAg, it becomes apparent that even freezing a couple of core orbitals reduces the accuracy of W_d significantly. This is way less so for YbAu, where freezing almost 20 percent of the core electrons only reduces W_d by 0.38 percent. Another difference that can be observed for YbAu compared to the other two molecules is that W_d actually increases once

when reducing the number of correlated electrons. When freezing 82 electrons, W_d is less than two percent smaller than when correlating all electrons, while when freezing 56 electrons, W_d is around six percent smaller. Since the computations are a lot less complex for the cut-off at ±10 a.u. and the result is not too much affected, this cut-off will be used for the final calculation of W_d for YbAu.

TABLE 7. The eEDM enhancement factor of YbAu computed while freezing a different number of orbitals. The W_d values were computed using the FSCCSD method, a 4c Hamiltonian and a v2z basis set. N_{elec}^{corr} is the number of correlated electrons and N_{elec}^{total} is the total number of electrons in the system. The final column gives the relative difference of W_d compared to correlating all electrons.

Active(−)/virtual(+) space cut-off [a.u.]	N_{elec}^{corr}	$\frac{N_{elec}^{corr}}{N_{elec}^{total}}$	Frozen orbitals Yb	Au	W_d $\left[10^{24}\frac{\text{h Hz}}{\text{e cm}}\right]$	Difference [%]
±2.68	35	0.2349	[Kr]4d^{10}	[Xe]4f^{14}	1.071	-34.18
±10	67	0.4527	[Kr]	[Kr]4d^{10}	1.595	-1.91
±40	93	0.6284	[Ar]3d^{10}	[Ar]3d^{10}	1.532	-5.81
±95	121	0.8176	[Ne]	[Ne]	1.620	-0.38
±3000	149	1	-	-	1.626	-

To better understand the similarities and differences between the three molecules regarding electron correlation, Figure 7 shows how W_d varies with increasing amount of frozen orbitals for YbCu, YbAg and YbAu. From this figure, it is obvious that the dependence of W_d on the amount of correlated electrons is comparable for YbCu and YbAg. However, YbAu shows a different trend, since there, freezing the core orbitals seems to leave W_d mostly invariant and W_d does not always increase when correlating more orbitals. This discrepancy could be due to effects such as screening and is dependent on the type of orbitals that are added.

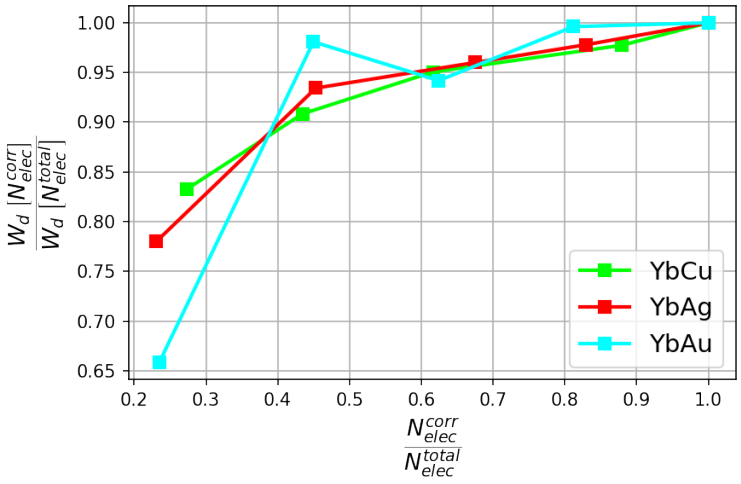

FIGURE 7. The effect of freezing orbitals on W_d for YbCu, YbAg and YbAu. The vertical axis represents the fraction of W_d compared to W_d computed with all electrons correlated. The horizontal axis represents the fraction of correlated electrons.

4.3.2. **Virtual space cut-off.** While in the last subsection, the active space cut-off was varied to observe the effects of freezing active orbitals, here the virtual space cut-off will be varied. This in turn

means that the dependency of W_d on the amount of available virtual orbitals will be investigated. For these computations, the FSCCSD method, a 4c Hamiltonian and a v2z basis set will be utilized, and all electrons will be correlated. This means that the active space cut-off was set to -2500 a.u. for YbCu and YbAg, and to -3000 a.u. for YbAu.

In Table 8, the results of varying the virtual space cut-off can be found for all three molecules. Similarly to what was observed in the previous subsection, the trends for YbCu and YbAg are comparable, while YbAu shows different behaviour.

For YbCu and YbAg, W_d increases as the number of virtual orbitals increases. However, for YbAu, W_d does not always increase when increasing the number of virtual orbitals. This becomes especially obvious when looking at the virtual space cut-off at 10 a.u.. There, the found W_d value is less than half a percent lower than the value found with a virtual space cut-off at 6000 a.u., while this difference can get up to six percent when including more virtual orbitals.

As the virtual space cut-off increases, the virtual orbitals are spread out more, which explains the small differences between W_d for a virtual space cut-off of 3000 and 6000. Furthermore, this is the reason for the results at a virtual space cut-off of 2500 and 3000 being equal. For both computations, the same amount of virtual orbitals were used. This can be seen from the number of virtual orbitals, N_V, that is given in Table 8.

TABLE 8. The eEDM enhancement factor W_d $\left[10^{24}\frac{\text{h Hz}}{\text{e cm}}\right]$ of YbCu, YbAg and YbAu computed for a variety of virtual space cut-off values. The number of virtual orbitals, N_V, is given for each cut-off value. The computations were performed using the FSCCSD method, a 4c Hamiltonian, a v2z basis set and by correlating all electrons. The relative difference of W_d compared to a virtual space cut-off of 6000 is given for each molecule.

	YbCu			YbAg			YbAu		
Virtual space cut-off [a.u.]	N_V	W_d	%	N_V	W_d	%	N_V	W_d	%
10	200	12.029	-6.31	210	11.037	-6.22	214	1.631	-0.30
30	262	12.368	-3.67	274	11.338	-3.66	292	1.547	-5.47
100	310	12.517	-2.52	322	11.472	-2.52	354	1.538	-6.00
500	380	12.694	-1.13	392	11.637	-1.12	462	1.615	-1.29
1000	406	12.757	-0.64	428	11.696	-0.62	488	1.614	-1.37
2000	424	12.769	-0.55	446	11.704	-0.56	530	1.605	-1.90
2500	432	12.803	-0.29	464	11.737	-0.27	538	1.626	-0.61
3000	432	12.803	-0.29	464	11.737	-0.27	538	1.626	-0.61
6000	446	12.840	-	486	11.769	-	570	1.636	-

To better see the differences and similarities between the three molecules in terms of the virtual space cut-off, Figure 8 is instructive. It becomes clear that the dependency of the virtual space cut-off on W_d is almost identical for YbCu and YbAg. The different behaviour observed for YbAu could be due to different types of virtual orbitals being included.

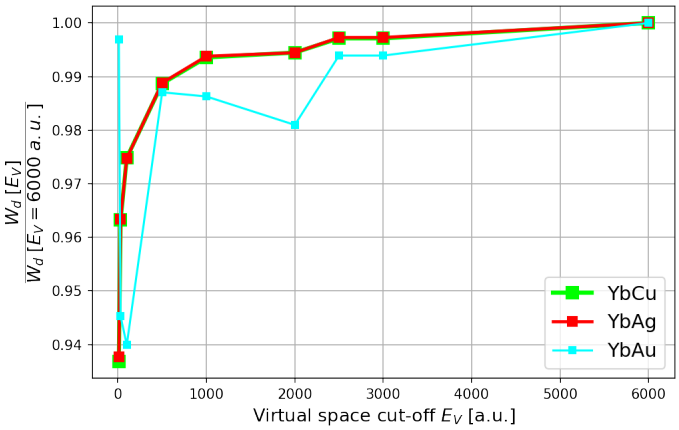

FIGURE 8. The effect of the virtual space cut-off on W_d for YbCu, YbAg and YbAu. The vertical axis represents the fraction of W_d compared to W_d computed at a virtual space cut-off of 6000 a.u..

4.4. **Basis set.** Now the effects of electron correlation on W_d are known, those results can be used to observe the effects of changing the used basis set. Computations with all electrons correlated are not feasible for quadruple zeta basis sets. So instead, to investigate the effects of the basis set on W_d, the active and virtual space cut-offs were set to ±20 a.u., ±10 a.u. and ±10 a.u. for YbCu, YbAg and YbAu, respectively. From Table 5 and Table 6, it can be observed that this reduces the accuracy of W_d by around five to six percent for YbCu and YbAg. The reduction should not affect the computations with different basis sets, as it is assumed that the different computational aspects are decoupled, since they are higher order terms. For the computations with different basis sets, the FSCCSD method and a 4c Hamiltonian were used.

TABLE 9. The eEDM enhancement factor W_d of YbCu, YbAg and YbAu for valence, core-valence and single augmented basis sets of second, third and fourth-order. Computations were done with the FSCCSD method and a 4c Hamiltonian. The virtual and active space cut-offs were set to ±20 a.u., ±10 a.u. and ±10 a.u., freezing 38, 64 and 82 electrons of YbCu, YbAg and YbAu, respectively.

YbCu				YbAg			
	$W_d\ \left[10^{24}\frac{\text{h Hz}}{\text{e cm}}\right]$				$W_d\ \left[10^{24}\frac{\text{h Hz}}{\text{e cm}}\right]$		
X	vXz	cvXz	s-aug-vXz	X	vXz	cvXz	s-aug-vXz
2	12.169	12.169	12.207	2	10.966	10.967	10.947
3	12.594	12.594	12.593	3	11.158	11.159	11.153
4	12.614	-	-	4	11.193	-	-

YbAu			
	$W_d\ \left[10^{24}\frac{\text{h Hz}}{\text{e cm}}\right]$		
X	vXz	cvXz	s-aug-vXz
2	1.595	1.596	1.492
3	1.122	1.127	1.089
4	1.314	-	-

In Table 9, the results of the computations using various basis sets can be found for all three molecules. Computations were done with basis sets with different cardinality, so the v2z, v3z and v4z basis sets. Furthermore, diffuse and tight functions were added to the v2z and v3z basis set to see the effects of adding functions to specific regions in the system.

The computations with added tight and diffuse functions were not performed on the quadruple zeta level, since these computations were too computationally demanding. Furthermore, the triple zeta results already are accurate enough to be used for uncertainty estimation.

Table 9 shows that, for YbCu and YbAg, W_d increases with increasing cardinality of basis set. However, the increase does flatten and will reach the CBS limit. The cv3z results only differ slightly from the v3z results, since these basis sets use the same functions for the ytterbium atom and only add a single tight function for the Cu atom and three tight functions for the Ag atom. Augmenting diffuse functions to the basis sets also does not change W_d significantly for both molecules. Although, adding diffuse functions does alter the value more than adding tight functions. The behaviour is different for YbAu, W_d first decreases when going to the v3z basis set, but then increases again when going to the v4z basis set. Again, the amount by which the W_d results differ decreases for increasing cardinality, showing the convergence to the CBS limit. The cv3z basis set yields a different result for YbAu. This basis set adds 3 tight functions to the v3z basis set. Augmenting diffuse functions has an even larger effect on W_d as can be seen from the s-aug-v3z result.

4.5. **Method and relativity.** Only from the fact that the three systems that are covered in this thesis have an open shell, the FSCCSD method should describe the system the best. Still, it is insightful to observe the results computed with different methods. In Section 3.6, the DHF, MP and CC methods were introduced, and these methods were used to compute W_d along with FSCCSD. For these computations, the v3z basis set was used and the virtual and active space cut-offs were set to ± 20 a.u., ± 30 a.u. and ± 10 a.u., freezing 38, 38 and 82 electrons of YbCu, YbAg and YbAu, respectively. The results of these calculations can be found in Table 10.

TABLE 10. The eEDM enhancement factor W_d of YbCu, YbAg and YbAu computed with the Dirac-Hartree-Fock method, Møller–Plesset perturbation theory and coupled cluster approaches. Computations were done with the v3z basis set and the virtual and active space cut-offs were set to ± 20 a.u., ± 30 a.u. and ± 10 a.u., freezing 38, 38 and 82 electrons of YbCu, YbAg and YbAu, respectively.

	YbCu	YbAg	YbAu
Method	$W_d \left[10^{24} \frac{\text{h Hz}}{\text{e cm}}\right]$	$W_d \left[10^{24} \frac{\text{h Hz}}{\text{e cm}}\right]$	$W_d \left[10^{24} \frac{\text{h Hz}}{\text{e cm}}\right]$
4c-DHF	9.763	9.502	7.379
4c-MP2	12.169	11.709	6.599
4c-CCSD	13.602	12.483	1.780
4c-CCSD + T	12.423	11.444	-1.062
4c-CCSD(T)	13.011	12.045	3.672
4c-CCSD − T	13.011	11.964	2.819
4c-FSCCSD	12.594	11.383	1.325

This table shows that, again, YbCu and YbAg behave similarly. The DHF results are underestimated, since electron correlation is not taken into account. Furthermore, the CC and MP2 results are all of similar magnitude. The extra fifth-order perturbation term that CCSD − T adds to CCSD(T) does not seem to influence the result for the YbCu molecule, while it does change W_d

for the other two molecules. The behaviour of YbAu is very sporadic. This could be due to YbAu being a large system, gold being very electronegative, gold being the heavier atom in that molecule, or a combination of these factors. Furthermore, these systems are open-shell systems and therefore, the CC method will not always give accurate results, unlike the FSCCSD method. This could also explain the behaviour that is observed for YbAu.

Apart from the method, the treatment of relativity can also be varied. The 4c Hamiltonian, used so far, does not treat relativity completely. It is missing both the Breit term and the QED effects. Currently, it is only possible to add the Gaunt term to the 4c Hamiltonian. Furthermore, this functionality can, as of now, only be added to the DHF method and not to a CC method. So, to observe the effect of the Gaunt term, computations were done with the DHF method, the v2z basis set and the virtual and active space cut-offs at ±20 a.u., ±30 a.u. and ±10 a.u., freezing 38, 38 and 82 electrons of YbCu, YbAg and YbAu, respectively. The results can be found in Table 11. The Gaunt term reduces the found W_d values for all three molecules when computed with the DHF method. It is not possible to investigate other relativistic effects currently, so this will be taken into account for the uncertainty as described in Section 4.7.

TABLE 11. The eEDM enhancement factor W_d of YbCu, YbAg and YbAu computed with the four component Hamiltonian and with the Gaunt term added to the Dirac Hamiltonian. Computations were done with the Dirac-Hartree-Fock method, the v2z basis set and the virtual and active space cut-offs were set to ±20 a.u., ±30 a.u. and ±10 a.u., freezing 38, 38 and 82 electrons of YbCu, YbAg and YbAu, respectively.

	YbCu	YbAg	YbAu
Method	$W_d \left[10^{24} \frac{\text{h Hz}}{\text{e cm}}\right]$	$W_d \left[10^{24} \frac{\text{h Hz}}{\text{e cm}}\right]$	$W_d \left[10^{24} \frac{\text{h Hz}}{\text{e cm}}\right]$
4c-DHF	9.562	9.350	7.233
4c-DHF + ΔGaunt	9.389	9.179	7.096

4.6. **Geometry.** So far, all computations have been performed with the geometry that was found in Section 4.1. However, it is not known how accurate these found values are. Usually, the computed value is compared to a value found experimentally, but such a value has not been determined for the three molecules covered in this thesis. Changing the geometry of the system will affect the found value of W_d. So, the uncertainty in R_e should be taken into account for the uncertainty in W_d as detailed in Section 4.7. To circumvent the issue of not having an experimental optimal geometry, the usual difference between computation and experiment will be used. Generally, this difference is around 0.01 Å [66].

TABLE 12. The eEDM enhancement factor W_d of YbCu, YbAg and YbAu for three different geometries computed with the FSCCSD method, a 4c Hamiltonian and the v3z basis set and the virtual and active space cut-offs were set to ±20 a.u., ±30 a.u. and ±10 a.u., freezing 38, 38 and 82 electrons of YbCu, YbAg and YbAu, respectively. The |Δ| columns give the absolute difference with respect to W_d found with R_e.

	YbCu		YbAg		YbAu	
Distance [Å]	$W_d \left[10^{24} \frac{\text{h Hz}}{\text{e cm}}\right]$	|Δ|	$W_d \left[10^{24} \frac{\text{h Hz}}{\text{e cm}}\right]$	|Δ|	$W_d \left[10^{24} \frac{\text{h Hz}}{\text{e cm}}\right]$	|Δ|
-0.01	12.569	0.025	11.366	0.016	1.201	0.080
0.00	12.594	-	11.383	-	1.122	-
0.01	12.618	0.024	11.398	0.015	1.041	0.081

Thus, computations of W_d were done for all three molecules, both adding and subtracting 0.01 Å from the optimal geometries. For these computations, the FSCCSD method, a 4c Hamiltonian and the v3z basis set were used. The virtual space cut-off was set to 20 a.u., 30 a.u. and 10 a.u. for YbCu, YbAg and YbAu, respectively. 38 electrons were frozen for YbCu, 38 electrons were frozen for YbAg and 82 electrons were frozen for YbAu. The results can be found in Table 12.

From the table, it becomes clear that changing the geometry slightly has a significant impact on W_d. Especially for YbAu, where the relative difference is over seven percent. Furthermore, it can be observed that W_d changes linearly with changing bond distance. So, the W_d uncertainty has about the same magnitude for positive and negative geometry changes. The results of this table will be used in the uncertainty analysis of Section 4.7.

4.6.1. **Vibrational correction.** Apart from the uncertainty in R_e, another geometrical contribution has to be taken into account. Introduced in Section 3.7, the vibrational correction should be added as an uncertainty. This correction comes from the fact that the electron's potential energy curve is anharmonic. So the averaged out W_d value will not be at the equilibrium bond length. By determining W_d and the total molecular energy at various bond lengths, the vibrational correction can be computed. This was done using a built-in program from DIRAC that computes the value of W_d in the lowest vibrational state and gives the difference compared to the value found at R_e. The values used as input for the program can be found in Table 13.

TABLE 13. The eEDM enhancement factor W_d and molecular energy of YbCu, YbAg and YbAu computed for various bond lengths. Computations were done with the FSCCSD method, the v3z basis set and the virtual and active space cut-offs were set to ±20 a.u., ±30 a.u. and ±10 a.u., freezing 38, 38 and 82 electrons of YbCu, YbAg and YbAu, respectively.

YbCu		
Bond length	Energy [a.u.]	W_d $\left[10^{24}\frac{\text{h Hz}}{\text{e cm}}\right]$
2.6543	-15724.627782	12.820
2.7043	-15724.628247	12.712
2.7443	-15724.628390	12.619
2.7543	-15724.628397	12.594
2.7643	-15724.628393	12.569
2.8043	-15724.628277	12.466
2.8543	-15724.627926	12.327

YbAg		
Bond length	Energy [a.u.]	W_d $\left[10^{24}\frac{\text{h Hz}}{\text{e cm}}\right]$
2.7589	-19386.073785	11.515
2.8089	-19386.074365	11.455
2.8489	-19386.074578	11.398
2.8589	-19386.074601	11.383
2.8689	-19386.074611	11.366
2.9089	-19386.074545	11.296
2.9589	-19386.074243	11.197

YbAu		
Bond length	Energy [a.u.]	W_d $\left[10^{24}\frac{\text{h Hz}}{\text{e cm}}\right]$
2.5524	-33108.669491	0.228
2.6024	-33108.670891	0.700
2.6424	-33108.671462	1.041
2.6524	-33108.671537	1.122
2.6624	-33108.671587	1.201
2.7024	-33108.671549	1.497
2.7524	-33108.671031	1.824

Table 13 shows that W_d decreases with increasing bond length for YbCu and YbAg, while it increases with increasing bond length for YbAu. This means that, due to the anharmonicity of the potential energy curve, W_d is shifted downward for YbCu and YbAg, and shifted upward for YbAu. Furthermore, it can be observed that for YbAg and YbAu, the lowest energy does not occur at the previously defined optimal geometry. This is due to the energy now being calculated using the FSCCSD method and the v3z basis set instead of the CCSD method with the s-aug-v4z basis set. For YbCu, the optimal geometries just happen to be equal when computed with both methods.

The found vibrational corrections are $-0.0322 \cdot 10^{24} \frac{\text{h Hz}}{\text{e cm}}$, $-0.0235 \cdot 10^{24} \frac{\text{h Hz}}{\text{e cm}}$ and $0.0130 \cdot 10^{24} \frac{\text{h Hz}}{\text{e cm}}$ for YbCu, YbAg and YbAu, respectively. By making a linear fit for the W_d data points against the bond length, the effective equilibrium bond distance can be found. This value was found to be 2.7643 Å for YbCu, 2.8676 Å for YbAg and 2.6583 Å for YbAu. These averaged-out values are plotted together with the relation between W_d and the bond length in Figure 9. This figure also shows that a linear relation is not optimal, as there is a slight parabolic shape discernable in the data points.

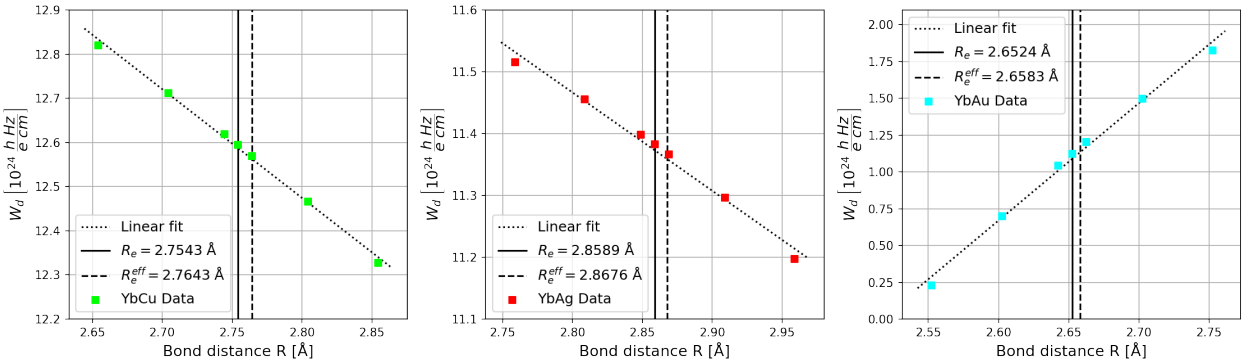

FIGURE 9. The effect of the bond distance on W_d for YbCu, YbAg and YbAu. A linear fit is given, along with the equilibrium bond distance and the effective equilibrium bond distance, given by the averaged out value in the vibrational ground state.

4.7. **Uncertainty.** Arguably more important than the absolute values of the results is the accuracy of the results. So, in this section, possible sources of uncertainty will be investigated. These uncertainties will be combined to yield the final uncertainty of W_d for YbCu, YbAg and YbAu. The sources of uncertainty fall under one of the following four main categories: basis set, electron correlation, relativity and geometry. Many of these topics have already been discussed in previous sections.

The used reference values try to find the middle ground between the different computation considerations. The calculations will be performed at the equilibrium bond distance that was optimized in Section 4.1. The other computational consideration employed for the reference values can be found in Table 14. A significant amount of orbitals was frozen for each molecule to reduce computational complexity. The cut-offs were set to ±10 for YbAu, since there the difference compared to correlating all electrons was smaller than the results with larger cut-offs. Since the cut-offs were smaller for YbAu, it was possible to perform a v4z calculation for W_d, while for the other two molecules with the larger amount of correlated electrons, only a v3z basis set was feasible. All the W_S computations were performed with a v3z basis set due to time constraints.

TABLE 14. The computational considerations used to determine the reference values of W_d and W_S for YbCu, YbAg and YbAu.

W_d					
Molecule	Method	Hamiltonian	Basis set	Active space cut-off	Virtual space cut-off
YbCu	FSCCSD	4c	v3z	-100 a.u.	100 a.u.
YbAg	FSCCSD	4c	v3z	-100 a.u.	100 a.u.
YbAu	FSCCSD	4c	v4z	-10 a.u.	10 a.u.
W_S					
Molecule	Method	Hamiltonian	Basis set	Active space cut-off	Virtual space cut-off
YbCu	FSCCSD	4c	v3z	-100 a.u.	100 a.u.
YbAg	FSCCSD	4c	v3z	-100 a.u.	100 a.u.
YbAu	FSCCSD	4c	v3z	-10 a.u.	10 a.u.

First, the uncertainty in the chosen basis set. There are three sources of basis set uncertainty. The best way to describe orbitals would be with an infinite number of Gaussians per orbital, giving the complete basis set. For YbCu and YbAg, the general quality of the used basis set is determined by the difference between the v4z basis set and the used v3z basis set, plus half of that difference for all larger basis sets. Since for YbAu, the v4z basis set is used for the reference values, its uncertainty in the general basis set quality is half the difference between the used v4z basis set and the v3z basis set. Apart from general basis set quality, also the effect of adding tight and diffuse functions was determined in Section 4.4. The uncertainty in tight functions will be given by the difference between the cv3z result and the v3z result, and the uncertainty in diffuse functions will be given by the difference between the s-aug-v3z result and the v3z result. Combining these three sources of uncertainty yields the total basis set uncertainty.

Second, the uncertainty in the electron correlation. To reduce the computational costs of the calculation, some orbitals were frozen in the computation of W_d. The difference between W_d found with freezing orbitals and W_d found with correlating all electrons gives this uncertainty. Furthermore, the virtual space cut-off still affects W_d beyond the values that were used for correlating all electrons. The uncertainty in the virtual space cut-off will be given by the difference in W_d found for a virtual cut-off at 6000 a.u. and 2500 a.u. for YbCu and YbAg, or 3000 a.u. for YbAu. Combining these factors yields a large uncertainty in the values regarding electron correlation. Moreover, higher excitation should also be taken into account, since the performed calculations only account for single and double excitations. Currently, there is no way to perform higher excitation calculations using the Fock space method, this means that this error cannot be accurately determined. Instead, to cover this source of error, twice the difference between the CCSD and the CCSD(T) result was taken as the uncertainty in higher excitations. The factor of two is there, since not all triple excitations are included in the CCSD(T) method.

Third, the uncertainty in the treatment of relativity. For the final computation, a 4c Hamiltonian was used, which treats relativity fairly well. However, from Section 3.3, it is known that adding the Breit term would increase accuracy, and for a full treatment, QED effects should also be taken into account. So, the value that will be used for the uncertainty is two times the difference between the 4c-DHF + ΔGaunt and the 4c-DHF result. Where the factor two covers the Gaunt term, the Gauge term and the QED interactions. It is assumed that the Gauge term and the QED effects are smaller than the Gaunt contribution. This same scheme was used for the determination of relativity

uncertainty for BaF [5]. Currently, the Gaunt term can only be incorporated in the computations at the DHF level, which is why DHF results are used instead of FSCCSD results.

Finally, the uncertainty in the used geometry. In this thesis, the geometry of the molecules was optimized. However, there is still an error in the optimal geometry. Thus, a separate calculation was done with geometries $R-\delta R$ and $R+\delta R$ in Section 4.6. Then the difference in found W_d gives the uncertainty. Also, the vibrational effects treated in the previous section have to be accounted for, so that uncertainty is added as well.

All the uncertainties mentioned so far have to be combined. This is done assuming that the errors are independent, which they will most likely not be entirely. This assumption is still valid, since most of the errors will be overestimated and all the mentioned effects are higher order effects. To combine the individual errors, they will be squared and then summed. Afterwards, the square root will be taken to find the full uncertainty. The results of the error analysis can be found in Table 15.

TABLE 15. The various sources of uncertainty for W_d of YbCu, YbAg and YbAu. The uncertainties are assumed to be independent, and the total uncertainty is given accordingly.

Source of uncertainty	Estimation scheme	δW_d $\left[10^{24}\frac{\text{h Hz}}{\text{e cm}}\right]$		
		YbCu	YbAg	YbAu
Basis set				
Basis set quality	$3/2 \cdot (\text{v4z} - \text{v3z}) \vee (\text{v4z} - \text{v3z})/2$	0.030	0.053	0.097
Diffuse functions	s-aug-v3z − v3z	0.002	0.005	0.033
Tight functions	cv3z − v3z	0.0002	0.0014	0.0050
Electron correlation				
Freezing orbitals	Difference to all electron	0.291	0.260	0.032
Virtual space cut-off	6000 a.u. − 3000 a.u.	0.037	0.032	0.010
Higher excitations	$2 \cdot (\text{CCSD(T)} - \text{CCSD})$	1.183	0.877	0.124
Relativity				
Breit term and QED	$2 \cdot (\text{DHF} - \text{DHF}+\Delta\text{Gaunt})$	0.347	0.342	0.274
Geometry				
R uncertainty	$R_e - (R_e - \delta R_e)$	0.013	0.017	0.081
Vibrational correction	$R_e - \nu_0$	0.033	0.024	0.013
Total uncertainty				
Absolute uncertainty	$\sum_i \sqrt{\delta_i}$	1.268	0.979	0.329
Relative uncertainty (%)		9.76	8.32	25.01

The uncertainty is also graphically displayed in Figure 10, where the individual contributions have been grouped according to the earlier defined main sources of uncertainty. Here it is already obvious that the uncertainty distribution varies for the three molecules. For YbCu and YbAg the uncertainty is mainly due to the treatment of electron correlation and especially not including higher excitations. Currently, adding higher excitations is not computationally possible with the FSCC method. For YbAu, the main source of uncertainty comes from not including relativistic effects such as the Breit term and QED effects. This uncertainty is also quite ill-defined, since only the influence of the

Gaunt term is known and assumptions for the magnitude of the Gauge term and QED effects were made to determine this uncertainty.

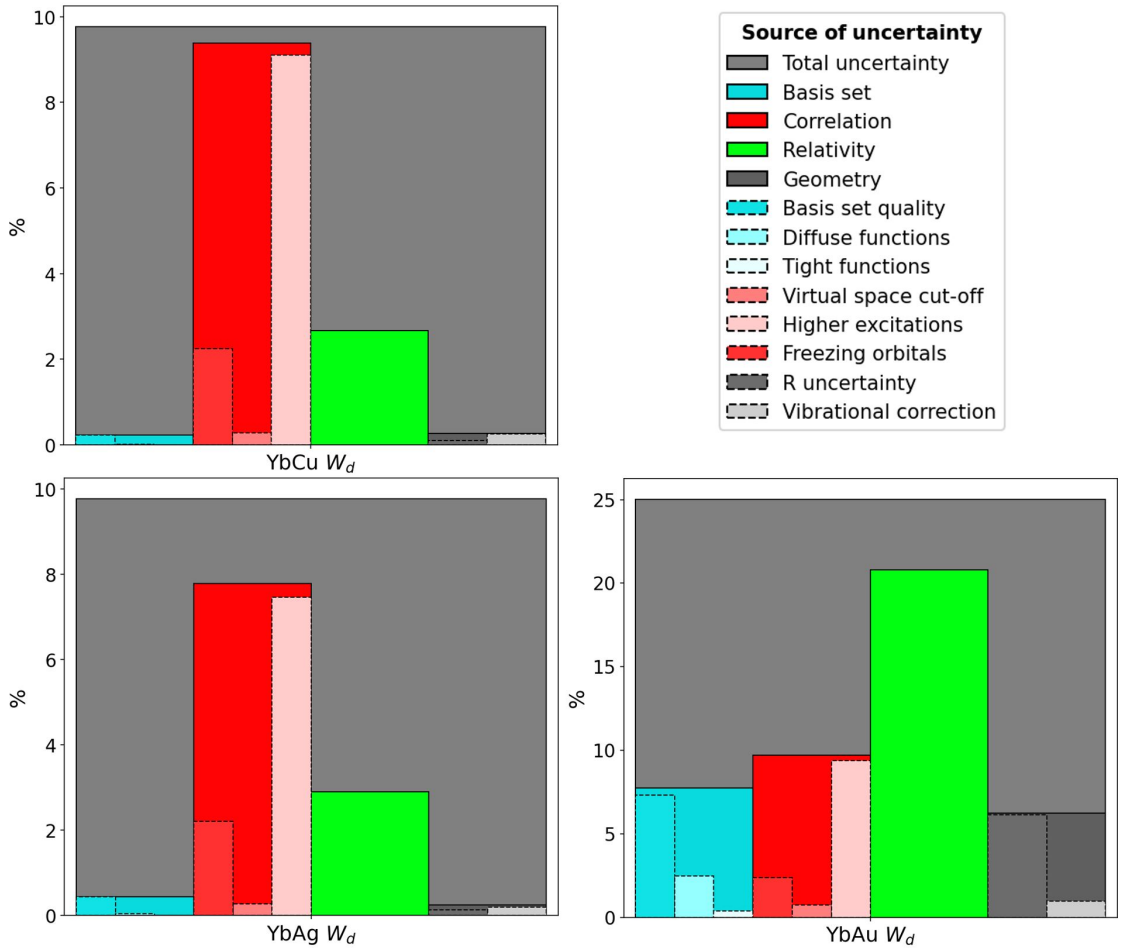

FIGURE 10. The relative uncertainty of W_d displayed as bar charts for YbCu, YbAg and YbAu. The individual sources of uncertainty are given as nested bar charts.

While Figure 10 displays the relative uncertainties compared to the found W_d value, Figure 11 shows more accurately how much each individual source of error contributes to the total uncertainty. The percentages are determined by dividing the square of the individual source of uncertainty by the square of the total uncertainty. Since the square of the individual contributions is used for determination of the uncertainty, sources that introduce slightly more uncertainty will contribute significantly more to the total uncertainty. For YbCu, not including higher excitations makes up 87 percent of the total uncertainty, while relativity only makes up 7.5 percent of the total uncertainty, even though the absolute uncertainty in relativity is only around three times smaller than that of not including higher excitations, as can be seen from Table 15.

The pie charts in Figure 11 show that the uncertainty of W_d for YbCu and YbAg is completely dominated by electron correlation and relativity treatment. While the uncertainty of W_d for YbAu is divided up between the four main sources of uncertainty. This uncertainty distribution that is seen for YbAu resembles similar uncertainty analyses from other papers [5, 67]. Thus, the uncertainty in electron correlation is most likely overestimated for YbCu and YbAg. This will be further discussed in Section 5.

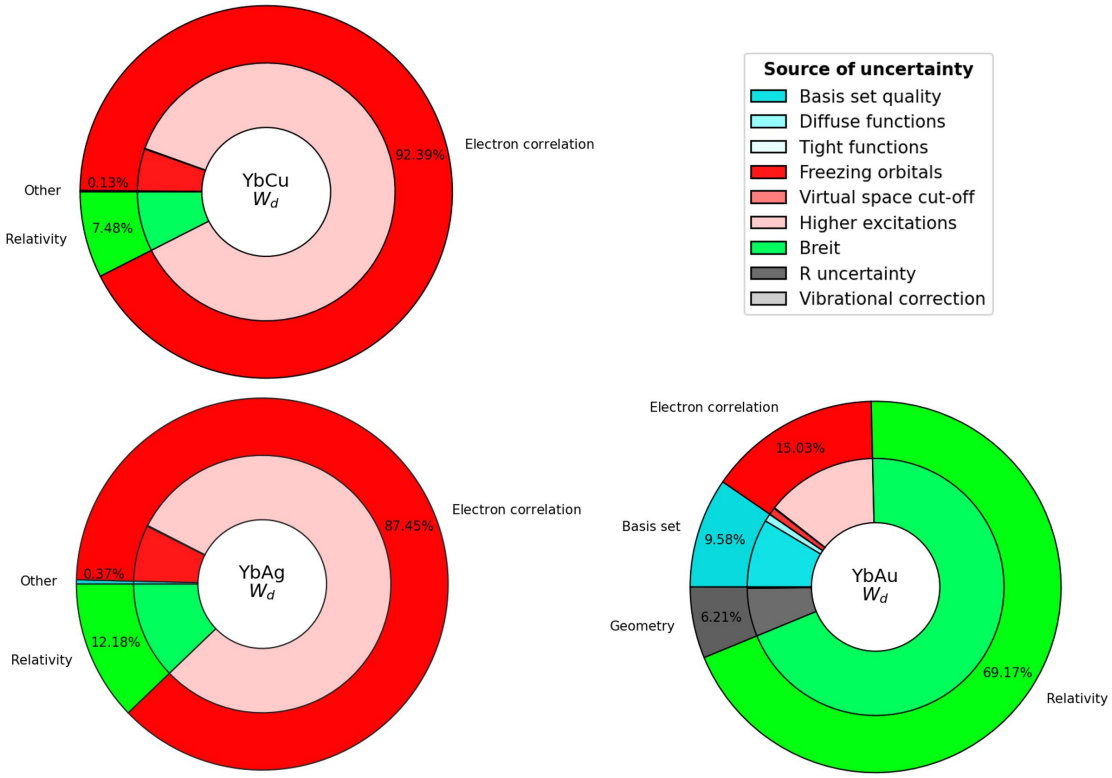

FIGURE 11. The distribution of all sources of uncertainty, given as a percentage of the total uncertainty of W_d for YbCu, YbAg and YbAu. The outer pie charts display the distribution of the four main uncertainty categories, while the inner pie charts display the distribution of the individual sources of uncertainty.

4.8. **Final Values.** In Table 16, the found values of W_d are given, along with the E_{eff}, the W_S values and the W_d to W_S ratio for YbCu, YbAg and YbAu. Only one calculation was performed for W_S to give an idea of its magnitude. The listed W_d uncertainty was computed in the previous section. The relative uncertainties found for W_d have been attributed to the W_S results. The uncertainties in E_{eff} and the W_d to W_S ratio were determined with the usual error analysis formulae [68]. The final W_d and W_S values were obtained with the computational considerations described in Table 14. In Section 5 these values will be compared to previously found values for other molecules.

TABLE 16. The eEDM enhancement factor W_d, effective electric field E_{eff}, S-PS interaction enhancement factor W_S and W_d to W_S ratio for YbCu, YbAg and YbAu. These values were computed using the FSCCSD method and a 4c Hamiltonian. All the W_d and W_S values were computed with the v3z basis set, except for the W_d value of YbAu, which was computed with the v4z basis set. The virtual and active space cut-offs were set to ±100 a.u., ±100 a.u. and ±10 a.u., freezing 12, 20 and 82 electrons of YbCu, YbAg and YbAu, respectively.

Molecule	W_d $\left[10^{24}\frac{\text{h Hz}}{\text{e cm}}\right]$	E_{eff} [GV cm^{-1}]	W_S [kHz]	$\frac{W_d}{W_S}$ $\left[10^{20}\frac{1}{\text{e cm}}\right]$
YbCu	12.98 ± 1.27	26.85 ± 2.63	67.0 ± 6.6	1.937 ± 0.268
YbAg	11.76 ± 0.98	24.31 ± 2.03	65.5 ± 5.5	1.794 ± 0.212
YbAu	1.31 ± 0.33	2.72 ± 0.68	63.3 ± 15.9	0.208 ± 0.074

5. **Discussion**

The final results found in this thesis do not mean much if they are not compared to other molecules. So, in Table 17 the found W_d and W_S values for YbCu, YbAg and YbAu are compared to values found for other molecules in other works. These other works use different computational considerations to compute the enhancement factors. Details on the used methods can be found in the sources listed in the table. The results for YbCu and YbAg are similar to the results found for other ytterbium-containing molecules, such as $YbCH_3$, YbF and YbOH. When switching out the heavier of the two atoms, for example, YbAg to RaAg, W_d and W_S change drastically. However, the ratio between the values stays consistent. Here again, it can be seen that W_d of YbAu does not seem to fit with results from other molecules, giving a quite unique W_d to W_S ratio. This might be of interest, since using a molecule with a different W_d to W_S ratio helps to disentangle the effects from the eEDM and S-PS interactions.

Apart from molecules that switch out one atom from the molecules investigated in this work, also BaF and ThO are listed. Currently, BaF is being used for eEDM searches at the Van Swinderen Institute in Groningen [9] and ThO was used to determine the current upper limit on the eEDM at Harvard-Yale [16]. The enhancement factors of the YbCu and YbAg molecules are higher than those of BaF, so in theory, they would be better candidates for eEDM searches, although practical limitations should still be taken into account. All the values found in this work are lower than the values found for ThO. This indicates that the molecules discussed in this work do not have extraordinarily high enhancement factors.

TABLE 17. The eEDM enhancement factor W_d, effective electric field E_{eff}, S-PS interaction enhancement factor W_S and W_d to W_S ratio for various molecules.

Molecule	Source	W_d $\left[10^{24}\frac{\text{h Hz}}{\text{e cm}}\right]$	E_{eff} [GV cm^{-1}]	W_S [h kHz]	$\frac{W_d}{W_S}$ $\left[10^{20}\frac{1}{\text{e cm}}\right]$
YbCu	This work	12.98	26.85	67.0	1.937
YbAg	This work	11.76	24.31	65.5	1.794
YbAu	This work	1.31	2.72	63.3	0.208
$YbCH_3$	[67]	13.80	28.54	45.97	3.00
YbF	[69] & [70]	11.64	24.07	41.2	2.83
YbOH	[12]	11.30	23.37	-	-
RaAg	[13]	32.0	66.1	181.1	1.77
BaF	[5]	3.13	6.47	8.29	3.78
ThO	[71]	20	84	116	1.7

In the previous section, the results of the W_d computations were given with their uncertainties. Throughout the process, many approximations had to be made to obtain the final results. To improve the accuracy of the found values, the following action can be taken in a future research. All of these possible improvements will assume more available computing power.

The most important aspect to include is full electron correlation. The amount of active orbitals that were frozen to obtain the values, increases the uncertainty significantly. It is recommended to perform these all electron computations with a symmetric virtual space cut-off, since Table 8 shows that W_d still has not converged for virtual space cut-offs below 2500 a.u.. Performing all electron calculations is feasible if more computing time is available. From Figure 11, it becomes

clear that correlation is the main contributor to the uncertainty of the W_d value. However, this large contribution is mainly due to the uncertainty in higher excitations. In this work, the FSCC method was chosen to compute the enhancement factors. This was done, since this method works better for open-shell molecules. Currently, it is not possible to add triple excitations to the FSCC method. So, to still get an idea of the uncertainty in higher excitations, the results from the regular CC method were used. However, since the regular CC method does not describe open-shell molecules well, the used uncertainty is not well based and most likely overestimated. Therefore, it is recommended to either establish a more accurate method of determining the uncertainty in higher excitations, or wait until triple excitations have been added to the FSCC method. One different approach used to determine the uncertainty in higher excitations is to take the difference between the results in the (0,1) sector and the (1,0) sector for FSCC [12].

The second-largest uncertainty in W_d comes from the treatment of relativity. In this thesis, a 4c Hamiltonian is used, but full relativity also requires the Breit term and QED effects to be taken into account. With the current version of DIRAC, it is not possible to add these terms to the FSCC Hamiltonian, so this improvement can not be implemented in the near future. However, more research could be done to investigate the relative sizes of these different relativistic contributions. This would help in determining the uncertainty in relativity more accurately.

Furthermore, the results in this work were computed with a triple or quadruple zeta basis set. To reduce the uncertainty in the general basis set quality, a higher order basis set could be utilized. Furthermore, the CBS limit could be determined and used as the reference value. Then the uncertainty would be due to the method used for CBS extrapolation. Apart from this improvement, tight and diffuse functions could be added to the basis set to improve the description of the system in those regions and reduce those errors as well. This will be of less importance than improving the description of electron correlation and relativity, since the uncertainty in the basis set is significantly smaller.

The final source of uncertainty comes from the geometry. The main point of contention is the different equilibrium bond lengths found in this work compared to the values found by Tomza in [24]. This discrepancy should be investigated further to understand which value to use for computing W_d and W_S.

Apart from more research to improve the accuracy of W_d, more time should be taken to perform a full uncertainty analysis for the S-PS interaction enhancement factor W_S. In this work, the relative error in W_d is attributed to W_S due to lack of time and resources. The uncertainty in W_S should be determined similarly to the uncertainty in W_d to produce more accurate results.

Another point of interest that has not been covered in this thesis is the large discrepancy between the W_d results of YbAu and the other two molecules. For most of the results, YbAu has shown different behaviour when changing the various computational parameters. Research should be done to understand the reason for YbAu behaving the way it does. The main differences of this molecule compared to the other two are that gold is more electronegative than both copper and silver. Furthermore, the YbAu molecule is quite special, since both atoms in the molecule are of similar mass. Moreover, since gold is a large atom, it also contains different orbitals. These differences could contribute to the discrepancy in W_d.

6. Conclusion

In this thesis, the eEDM enhancement factor W_d and the S-PS interaction enhancement factor W_S were calculated for the YbCu, YbAg and YbAu molecules. These values can be used to determine if the molecules are suitable for eEDM searches in future experiments. The uncertainty of the found W_d values was thoroughly investigated by identifying the possible sources of error, and the relative uncertainty was attributed to the W_S values.

To obtain the final results, the equilibrium bond length of the three ytterbium-containing molecules was optimized. With an s-aug-v4z basis set, the CCSD method and an X2c Hamiltonian, it was found that the optimal geometries are $R_e = 2.7543$ Å for YbCu, $R_e = 2.8589$ Å for YbAg and $R_e = 2.6524$ Å for YbAu.

The final results are: $W_d = 12.98 \pm 1.27 \cdot 10^{24} \frac{\text{h Hz}}{\text{e cm}}$ and $W_S = 67.0 \pm 6.6$ h kHz for YbCu, $W_d = 11.76 \pm 0.98 \cdot 10^{24} \frac{\text{h Hz}}{\text{e cm}}$ and $W_S = 65.5 \pm 5.5$ h kHz for YbAg, and $W_d = 1.31 \pm 0.33 \cdot 10^{24} \frac{\text{h Hz}}{\text{e cm}}$ and $W_S = 63.3 \pm 15.9$ h kHz for YbAu. All of these results were computed with the FSCCSD method, a 4c hamiltonian and a v3z basis set, apart from W_d for YbAu, which was computed with the FSCCSD method, a 4c hamiltonian and a v4z basis set. The virtual and active space cut-offs were set to ±100 a.u., ±100 a.u. and ±10 a.u., freezing 12, 20 and 82 electrons of YbCu, YbAg and YbAu, respectively. Further research can reduce the found uncertainties. This is especially true for the W_S values, since a full uncertainty analysis was not performed.

It is recommended to perform further computations with the three molecules covered in this work to refine the results. Especially a thorough uncertainty analysis of W_S would be beneficial. If practical limitations allow it, one of these molecules could be used to search for the eEDM in the future.

7. Acknowledgements

First and foremost, I would like to thank my supervisor Anastasia Borschevsky for coming up with an interesting project for my bachelor thesis and helping me out with the many questions I had on the theoretical part of this topic. I have enjoyed working on this paper, and I am interested to see where it will end up. Second, I highly appreciated all the time Yuly spent answering my many emails that I sent throughout the period. Apart from answering many technical questions, Yuly was also kind enough to submit some computations, such that they did not have to wait in the queue for days on end. Third, when writing this report, the master thesis by Diewertje Doeglas [72] has been really helpful for getting an idea of the topics that are covered in this field. Finally, I thank the Center for Information Technology of the University of Groningen for their support and for providing access to the Peregrine high performance computing cluster.

8. **Bibliography**

[1] M. S. Safronova, D. Budker, D. DeMille, Derek F. Jackson Kimball, A. Derevianko, and Charles W. Clark. "Search for new physics with atoms and molecules". In: *Reviews of Modern Physics* 90 (June 2018). DOI: 10.1103/revmodphys.90.025008.

[2] John Womersley and Fermilab. *Beyond the Standard Model*. Feb. 2005. URL: https://www.symmetrymagazine.org/article/february-2005/beyond-the-standard-model (visited on 05/02/2022).

[3] T. S. Virdee. "Beyond the standard model of particle physics". In: *Philosophical Transactions of the Royal Society A: Mathematical, Physical and Engineering Sciences* 374 (Aug. 2016), p. 20150259. DOI: 10.1098/rsta.2015.0259.

[4] Alan S. Cornell. "Some theories beyond the Standard Model". In: *Journal of Physics: Conference Series* 645 (Oct. 2015). DOI: 10.1088/1742-6596/645/1/012002.

[5] Pi A. B. Haase, Diewertje J. Doeglas, Alexander Boeschoten, Ephraim Eliav, Miroslav Iliaš, Parul Aggarwal, H. L. Bethlem, Anastasia Borschevsky, Kevin Esajas, Yongliang Hao, Steven Hoekstra, Virginia R. Marshall, Thomas B. Meijknecht, Maarten C. Mooij, Kees Steinebach, Rob G. E. Timmermans, Anno P. Touwen, Wim Ubachs, Lorenz Willmann, and Yanning Yin. "Systematic study and uncertainty evaluation of P, T-odd molecular enhancement factors in BaF". In: *The Journal of Chemical Physics* 155 (July 2021). DOI: 10.1063/5.0047344.

[6] Giacomo de Angelis. "The SPES radioactive ion beam facility at the Legnaro National Laboratories and the EDM search". In: *Journal of Physics: Conference Series* 1056 (July 2018). DOI: 10.1088/1742-6596/1056/1/012014.

[7] Brian R. Martin and Graham Shaw. *Nuclear and Particle Physics: An Introduction*. 3rd ed. John Wiley & Sons Ltd, 2019, pp. 244–246.

[8] Maxim Pospelov and Adam Ritz. "Electric dipole moments as probes of new physics". In: *Annals of Physics* 318 (July 2005), pp. 119–169. DOI: 10.1016/j.aop.2005.04.002.

[9] Van Swinderen Institute. *electron-EDM*. May 2021. URL: https://www-rug-nl.proxy-ub.rug.nl/research/vsi/newtopics/eedm?lang=en (visited on 05/02/2022).

[10] C. J. G. Onderwater. "Direct measurement of charged particle EDMs". In: International Conference on Exotic Atoms. Storage Ring EDM Collaboration. Vienna, Austria: Austrian Academy of Sciences Press, 2005. URL: https://austriaca.at/0xc1aa5576_0x000fd4e9.pdf (visited on 04/23/2022).

[11] Eugene D. Commins, J. D. Jackson, and David P. DeMille. "The electric dipole moment of the electron: An intuitive explanation for the evasion of Schiff's theorem". In: *American Journal of Physics* 75 (June 2007), pp. 532–536. DOI: 10.1119/1.2710486.

[12] Malika Denis, Pi A. B. Haase, Rob G. E. Timmermans, Ephraim Eliav, Nicholas R. Hutzler, and Anastasia Borschevsky. "Enhancement factor for the electric dipole moment of the electron in the BaOH and YbOH molecules". In: *Physical Review A* 99 (Apr. 2019). DOI: 10.1103/physreva.99.042512.

[13] Timo Fleig and David DeMille. "Theoretical aspects of radium-containing molecules amenable to assembly from laser-cooled atoms for new physics searches". In: *New Journal of Physics* 23 (Nov. 2021). DOI: 10.1088/1367-2630/ac3619.

[14] David DeMille. "Diatomic molecules, a window onto fundamental physics". In: *Physics Today* 68 (Dec. 2015), pp. 34–40. DOI: 10.1063/pt.3.3020.

[15] Mohit Verma, Andrew M. Jayich, and Amar C. Vutha. "Electron Electric Dipole Moment Searches Using Clock Transitions in Ultracold Molecules". In: *Physical Review Letters* 125 (Oct. 2020). DOI: 10.1103/physrevlett.125.153201.

[16] V. Andreev, D. G. Ang, D. DeMille, J. M. Doyle, G. Gabrielse, J. Haefner, N. R. Hutzler, Z. Lasner, C. Meisenhelder, B. R. O'Leary, C. D. Panda, A. D. West, E. P. West, X. Wu, and ACME Collaboration. "Improved limit on the electric dipole moment of the electron". In: *Nature* 562 (Oct. 2018), pp. 355–360. DOI: 10.1038/s41586-018-0599-8.

[17] Bertram M. Schwarzschild. "Surprising upper limit on the electron's electric dipole moment". In: *Physics Today* 67 (Apr. 2014), pp. 15–17. DOI: 10.1063/pt.3.2334.

[18] A. L. Allred. "Electronegativity values from thermochemical data". In: *Journal of Inorganic and Nuclear Chemistry* 17 (June 1961), pp. 215–221. DOI: 10.1016/0022-1902(61)80142-5.

[19] Gordon D. Sproul. "Evaluation of Electronegativity Scales". In: *ACS Omega* 5 (May 2020), pp. 11585–11594. DOI: 10.1021/acsomega.0c00831.

[20] H. S. Nataraj, B. K. Sahoo, B. P. Das, R. K. Chaudhuri, and D. Mukherjee. "The electron electric dipole moment enhancement factors of Rubidium and Caesium atoms". In: *Journal of Physics: Conference Series* 80 (Sept. 2007), p. 012050. DOI: 10.1088/1742-6596/80/1/012050.

[21] Konstantin Gaul, Sebastian Marquardt, Timur Isaev, and Robert Berger. "Systematic study of relativistic and chemical enhancements of $\mathcal{P}$, $\mathcal{T}$-odd effects in polar diatomic radicals". In: *Physical Review A* 99 (Mar. 2019). DOI: 10.1103/physreva.99.032509.

[22] Ann-Marie Mårtensson-Pendrill and Per Öster. "Calculations of atomic electric dipole moments". In: *Physica Scripta* 36.3 (Sept. 1987), pp. 445–446. DOI: 10.1088/0031-8949/36/3/011.

[23] Sudip Sasmal, Himadri Pathak, Malaya K. Nayak, Nayana Vaval, and Sourav Pal. "Search for parity and time reversal violating effects in HgH: Relativistic coupled-cluster study". In: *The Journal of Chemical Physics* 144 (Mar. 2016), p. 124307. DOI: 10.1063/1.4944673.

[24] Michał Tomza. "Interaction potentials, electric moments, polarizabilities, and chemical reactions of YbCu, YbAg, and YbAu molecules". In: *New Journal of Physics* 23.8 (Aug. 2021). DOI: 10.1088/1367-2630/ac1696.

[25] Timothy Chupp and Michael Ramsey-Musolf. "Electric dipole moments: A global analysis". In: *Physical Review C* 91 (Mar. 2015), p. 7. DOI: 10.1103/physrevc.91.035502.

[26] Takao Tsuneda. *Density Functional Theory in Quantum Chemistry*. 1st ed. Springer, Tokyo, 2014, pp. 35–59. ISBN: 978-4-431-54825-6.

[27] Wolfgang Demtröder. *Molecular Physics: Theoretical Principles and Experimental Methods*. John Wiley & Sons, 2005, pp. 20, 128. ISBN: 9783527405664.

[28] Trond Saue. "Relativistic Hamiltonians for Chemistry: A Primer". In: *ChemPhysChem* 12 (Nov. 2011), pp. 3077–3094. DOI: 10.1002/cphc.201100682.

[29] R. S. Mulliken. "Spectroscopy, Molecular Orbitals, and Chemical Bonding". In: *Science* 157 (July 1967), pp. 13–24. DOI: 10.1126/science.157.3784.13.

[30] David Tong. "Quantum Field Theory". In: *University of Cambridge Part III Mathematical Tripos* (2006). URL: https://www.damtp.cam.ac.uk/user/tong/qft/qft.pdf (visited on 05/01/2022).

[31] Frank Jensen. *Introduction to computational chemistry*. New Jersey John Wiley & Sons Inc, 2017. ISBN: 9781118825990.

[32] Wenjian Liu. "Ideas of relativistic quantum chemistry". In: *Molecular Physics* 108 (May 2010), pp. 1679–1706. DOI: 10.1080/00268971003781571.

[33] NIST. *CODATA Value: Hartree energy in eV*. July 2017. URL: https://physics.nist.gov/cgi-bin/cuu/Value?hrev (visited on 05/01/2022).

[34] C. David Sherrill. *Basis Sets in Quantum Chemistry*. Oct. 2008. URL: http://vergil.chemistry.gatech.edu/courses/chem6485/pdf/basis-sets.pdf (visited on 04/30/2022).

[35] Ernest R. Davidson and David Feller. "Basis set selection for molecular calculations". In: *Chemical Reviews* 86 (Aug. 1986), pp. 681–696. DOI: 10.1021/cr00074a002.

[36] Trygve Helgaker, Poul Jørgensen, and Jeppe Olsen. *Molecular Electronic-Structure Theory*. John Wiley & Sons Ltd, 2000, pp. 259–261. ISBN: 9781119019572. DOI: https://doi.org/10.1002/9781119019572.

[37] Frank Jensen. "Atomic orbital basis sets". In: *Wiley Interdisciplinary Reviews: Computational Molecular Science* 3 (Oct. 2012), pp. 273–295. DOI: 10.1002/wcms.1123.

[38] Frank Neese and Edward F. Valeev. "Revisiting the Atomic Natural Orbital Approach for Basis Sets: Robust Systematic Basis Sets for Explicitly Correlated and Conventional Correlated ab initio Methods?" In: *Journal of Chemical Theory and Computation* 7 (Dec. 2010), pp. 33–43. DOI: 10.1021/ct100396y.

[39] Kenneth G. Dyall. "Relativistic Double-Zeta, Triple-Zeta, and Quadruple-Zeta Basis Sets for the 4s, 5s, 6s, and 7s Elements". In: *The Journal of Physical Chemistry A* 113 (Aug. 2009), pp. 12638–12644. DOI: 10.1021/jp905057q.

[40] C. David Sherrill. *An Introduction to Hartree-Fock Molecular Orbital Theory*. June 2000. URL: http://vergil.chemistry.gatech.edu/notes/hf-intro/hf-intro.pdf (visited on 04/25/2022).

[41] Steven J. Leon. *Linear algebra with applications*. 9th ed. Pearson Education Limited, 2015, p. 113.

[42] C. K. Skylaris. *Experimental observables / Unpaired electrons*. University of Southampton, Oct. 2008. URL: https://www.southampton.ac.uk/assets/centresresearch/documents/compchem/chem3023_L8.pdf (visited on 05/24/2022).

[43] T. Daniel Crawford. *Size-Extensivity and Size-Consistency*. Jan. 1996. URL: https://web.archive.org/web/20170606215414/http://www.uam.es/docencia/quimcursos/Docs/Knowledge/Fundamental_Theory/cc/node7.html.

[44] Raymond F. Bishop and Hermann G. Kümmel. "The Coupled Cluster Method". In: *Physics Today* 40 (Mar. 1987), pp. 52–60. DOI: 10.1063/1.881103.

[45] Ira N. Levine. *Quantum chemistry*. Ed. by Adam Jaworski, Jeanne Zalesky, Jessica Moro, Lisa R. Pierce, Gina M. Cheselka, and Betty Pessagno. 7th ed. Pearson, 2014, pp. 546–552. ISBN: 978-0-321-80345-0.

[46] Lucas Visscher, Timothy J. Lee, and Kenneth G. Dyall. "Formulation and implementation of a relativistic unrestricted coupled-cluster method including noniterative connected triples". In: *The Journal of Chemical Physics* 105 (Nov. 1996), pp. 8769–8776. DOI: 10.1063/1.472655.

[47] A. Auer Alexander. *Coupled Cluster Theory and Tensor Decomposition Techniques*. Düsseldorf, Germany, Aug. 2011. URL: http://www-m3.ma.tum.de/foswiki/pub/M3/Allgemeines/MathChem/Talk_Auer2.pdf?t=12 (visited on 04/29/2022).

[48] John F. Stanton. "Why CCSD(T) works: a different perspective". In: *Chemical Physics Letters* 281 (Dec. 1997), pp. 130–134. DOI: 10.1016/s0009-2614(97)01144-5.

[49] R. J. Bartlett. "Many-Body Perturbation Theory and Coupled Cluster Theory for Electron Correlation in Molecules". In: *Annual Review of Physical Chemistry* 32 (Oct. 1981), pp. 359–401. DOI: 10.1146/annurev.pc.32.100181.002043.

[50] Uzi Kaldor. "The Fock space coupled cluster method: theory and application". In: *Theoretica Chimica Acta* 80 (1991), pp. 427–439. DOI: 10.1007/bf01119664.

[51] Soumi Haldar and Achintya Kumar Dutta. "An efficient Fock space multi-reference coupled cluster method based on natural orbitals: Theory, implementation, and benchmark". In: *The Journal of Chemical Physics* 155 (July 2021). DOI: 10.1063/5.0054171.

[52] Maria Barysz, Hendrik J. Monkhorst, and Leszek Z. Stolarczyk. "Fock-space coupled-cluster method". In: *Theoretica Chimica Acta* 80 (1991), pp. 483–507. DOI: 10.1007/bf01119667.

[53] Arie Landau, Ephraim Eliav, and Uzi Kaldor. "Intermediate Hamiltonian Fock-space coupled-cluster method". In: *Advances in Quantum Chemistry* 39 (2001), pp. 171–188. DOI: 10.1016/s0065-3276(05)39011-3.

[54] Leszek Meissner. "Various formulations of the Fock-space coupled-cluster method: Advantages and disadvantages in their practical implementations". In: *Chemical Physics* 401 (June 2012), pp. 136–145. DOI: 10.1016/j.chemphys.2011.09.012.

[55] Suhita Basumallick, Sourav Pal, and Mihai V. Putz. "Fock-Space Coupled Cluster Theory: Systematic Study of Partial Fourth Order Triples Schemes for Ionization Potential and Comparison with Bondonic Formalism". In: *International Journal of Molecular Sciences* 21 (Aug. 2020), p. 6199. DOI: 10.3390/ijms21176199.

[56] Nicholas D. K. Petraco, Ľuboš Horný, Henry F. Schaefer, and Ivan Hubač. "Brillouin–Wigner coupled cluster theory. Fock-space approach". In: *The Journal of Chemical Physics* 117 (Dec. 2002), pp. 9580–9587. DOI: 10.1063/1.1516802.

[57] Christopher J. Cramer. *Essentials of computational chemistry*. 2nd ed. John Wiley & Sons Ltd, 2004, pp. 219–222. ISBN: 9780470091814.

[58] Peter W. Atkins, Julio de Paula, and James Keeler. *Atkins' Physical Chemistry*. 11th ed. Oxford University Press, 2018, pp. 442–445. ISBN: 9780198769866.

[59] Davide Chicco, Matthijs J. Warrens, and Giuseppe Jurman. "The coefficient of determination R-squared is more informative than SMAPE, MAE, MAPE, MSE and RMSE in regression analysis evaluation". In: *PeerJ Computer Science* 7 (July 2021), pp. 2–5. DOI: 10.7717/peerj-cs.623.

[60] NIST. *CODATA Value: atomic unit of electric field*. 2018. URL: https://physics.nist.gov/cgi-bin/cuu/Value?auefld (visited on 06/01/2022).

[61] NIST. *CODATA Value: Planck constant in eV/Hz*. 2018. URL: https://physics.nist.gov/cgi-bin/cuu/Value?hev (visited on 06/01/2022).

[62] NIST. *CODATA Value: Planck constant*. 2018. URL: https://physics.nist.gov/cgi-bin/cuu/Value?h.

[63] NIST. *CODATA Value: atomic unit of energy*. 2018. URL: https://physics.nist.gov/cgi-bin/cuu/Value?Ahr (visited on 06/26/2022).

[64] DIRAC, a relativistic ab initio electronic structure program, Release DIRAC22, 2022, written by L. Visscher, H. J. Aa. Jensen, R. Bast, A. S. P. Gomes and T. Saue, with contributions from I. A. Aucar, V. Bakken, C. Chibueze, J. Creutzberg, K. G. Dyall, S. Dubillard, U. Ekström, E. Eliav, T. Enevoldsen, E. Faßhauer, T. Fleig, O. Fossgaard, L. Halbert, E. D. Hedegård, T. Helgaker, B. Helmich-Paris, J. Henriksson, M. van Horn, M. Iliaš, Ch. R. Jacob, S. Knecht, S. Komorovský, O. Kullie, J. K. Lærdahl, C. V. Larsen, Y. S. Lee, N. H. List, H. S. Nataraj, M. K. Nayak, P. Norman, M. Olejniczak, J. Olsen, J. M. H. Olsen, A. Papadopoulos, Y. C. Park, J. K. Pedersen, M. Pernpointner, J. V. Pototschnig, R. Di Remigio, M. Repisky, K. Ruud, P. Sałek, B. Schimmelpfennig, B. Senjean, A. Shee, J. Sikkema, A. Sunaga, A. J. Thorvaldsen, J. Thyssen, J. N. P. van Stralen, M. L. Vidal, S. Villaume, O. Visser, T. Winther, S. Yamamoto and X. Yuan. URL: http://www.diracprogram.org.

[65] R.J. Gillespie. "Fifty years of the VSEPR model". In: *Coordination Chemistry Reviews* 252 (July 2008), p. 1316. DOI: 10.1016/j.ccr.2007.07.007.

[66] Yongliang Hao, Lukáš F. Pašteka, Lucas Visscher, Parul Aggarwal, Hendrick L. Bethlem, Alexander Boeschoten, Anastasia Borschevsky, Malika Denis, Kevin Esajas, Steven Hoekstra, Klaus Jungmann, Virginia R. Marshall, Thomas B. Meijknecht, Maarten C. Mooij, Rob G. E. Timmermans, Anno Touwen, Wim Ubachs, Lorenz Willmann, Yanning Yin, and Artem Zapara. "High accuracy theoretical investigations of CaF, SrF, and BaF and implications for laser-cooling". In: *The Journal of Chemical Physics* 151 (July 2019). DOI: 10.1063/1.5098540.

[67] Yuly Chamorro, Anastasia Borschevsky, Ephraim Eliav, Nicholas R. Hutzler, and Lukáš F. Pašteka. "Molecular enhancement factors for P, T-violating eEDM in BaCH3 and YbCH3 symmetric top molecules" (2022). In preparation.

[68] R.J.H. Klein-Douwel. "Data and error analysis". In: University of Groningen, 2019. Chap. 2.2, p. 15.

[69] Malaya K. Nayak and Rajat K. Chaudhuri. "Re-appraisal of the P,T-odd interaction constant Wd in YbF: Relativistic configuration interaction approach". In: *Pramana* 73 (Sept. 2009), pp. 581–586. DOI: 10.1007/s12043-009-0110-z.

[70] Malaya K. Nayak, Rajat K. Chaudhuri, and B. P. Das. "Ab initio calculation of the electron-nucleus scalar-pseudoscalar interaction constant W_S in heavy polar molecules". In: *Physical Review A* 75 (Feb. 2007). DOI: 10.1103/physreva.75.022510.

[71] L. V. Skripnikov, A. N. Petrov, and A. V. Titov. "Communication: Theoretical study of ThO for the electron electric dipole moment search". In: *The Journal of Chemical Physics* 139 (Dec. 2013), p. 221103. DOI: 10.1063/1.4843955.

[72] Diewertje Doeglas. "Relativistic Coupled Cluster calculations of molecular properties of BaF and PbF required in high-precision experiments". MA thesis. University of Groningen, Jan. 2019.

Appendix A. Additional results

In this appendix, some tables and graphs can be found that support the results reported in Section 4. For the most part, these are results for YbAg and YbAu that are very similar to the results found for YbCu.

A.1. **Equilibrium bond length.** To compute the equilibrium bond distances of YbAg and YbAu, the potential energy curves from Figure 12 and Figure 13 were used. The data points were computed using the CCSD method, an X2c Hamiltonian and the s-aug-v4z basis set. The virtual space cut-off was set to 10 a.u., and 64 and 82 electrons were frozen for YbAg and YbAu, respectively. The minimum of the fourth order polynomial that was fit to the data points was used as the optimal geometry.

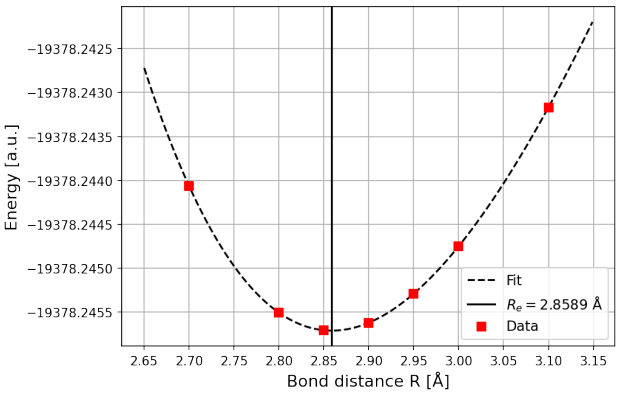

FIGURE 12. The potential energy curve of YbAg. The fit shown is a fourth-order polynomial. The minimum of this fit was chosen as the equilibrium bond distance R_e. The single-point energy calculations were performed using the CCSD method, an X2c Hamiltonian and the s-aug-v4z basis set. For the computations, 64 core electrons were frozen and the virtual space cut-off was set to 10 a.u..

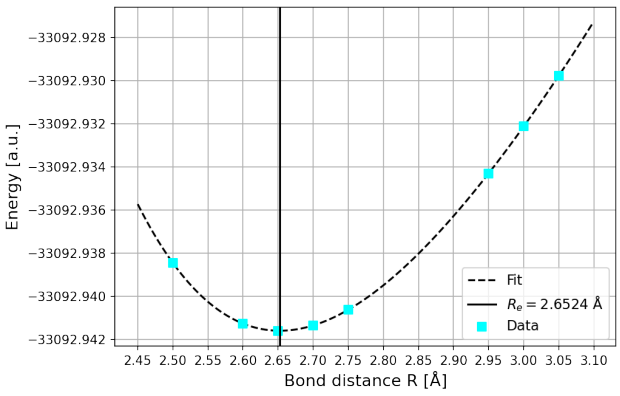

FIGURE 13. The potential energy curve of YbAu. The fit shown is a fourth-order polynomial. The minimum of this fit was chosen as the equilibrium bond distance R_e. The single-point energy calculations were performed using the CCSD method, an X2c Hamiltonian and the s-aug-v4z basis set. For the computations, 82 core electrons were frozen and the virtual space cut-off was set to 10 a.u..

A.2. **Field strength.** To determine the optimal field strength values for YbAg and YbAu, graphs similar to the ones displayed in Figure 5 were made for these two molecules. The graphs for YbAg can be found in Figure 14 and the graphs for YbAu can be found in Figure 15. The field strength computations were done using the CCSD method, a 4c Hamiltonian and the v2z basis set. The virtual space cut-off was set to 20 a.u. and 46 and 64 electrons were frozen for YbAg and YbAu, respectively. In the graphs for YbAu, it becomes clear that this molecule requires a lower field strength to adhere to the linear relation required for the finite field approach.

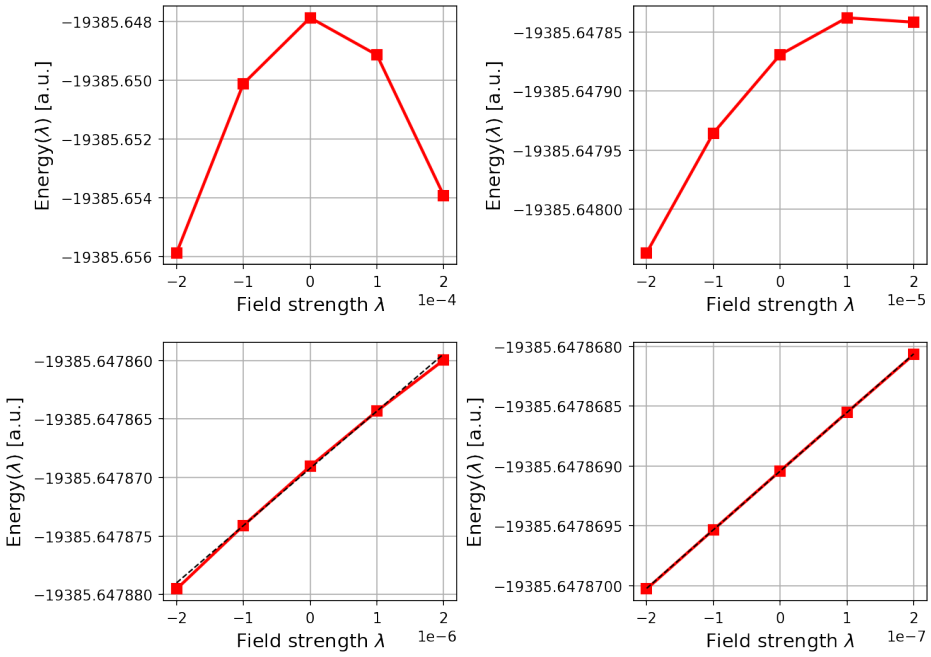

FIGURE 14. The dependence of the molecular energy of YbAg on the used field strength, using the optimized geometry, the v2z basis set, the CCSD method, a 4c Hamiltonian, a virtual space cut-off at 20 a.u. and freezing 46 core electrons. The dashed line shown in the bottom two plots represents a true linear relation.

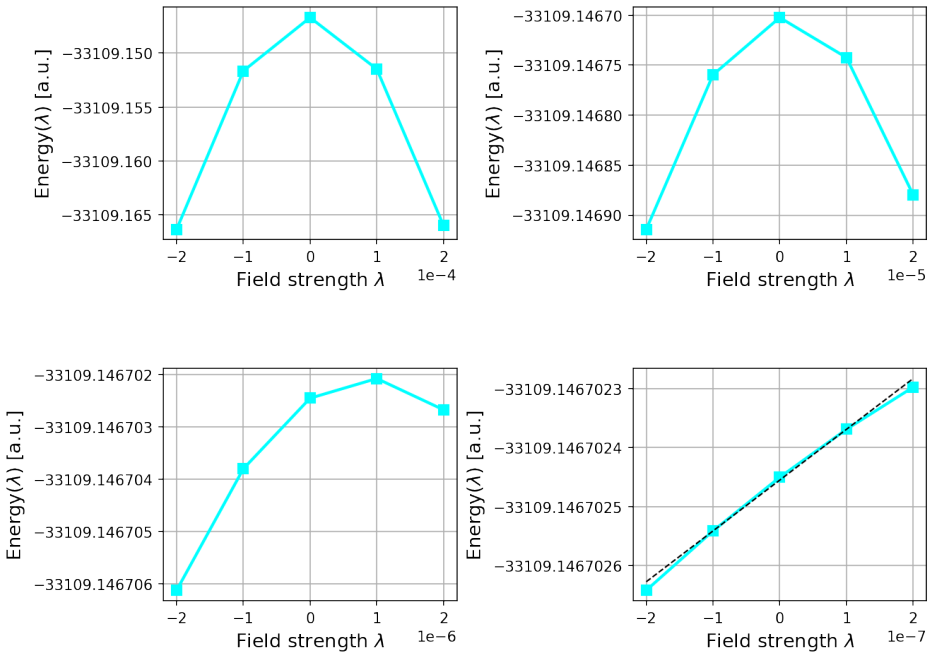

FIGURE 15. The dependence of the molecular energy of YbAu on the used field strength, using the optimized geometry, the v2z basis set, the CCSD method, a 4c Hamiltonian, a virtual space cut-off at 20 a.u. and freezing 64 core electrons. The dashed line shown in the bottom-right plot represents a true linear relation.

A.3. **Electron correlation.** Charts similar to Figure 6 for YbCu, can be seen in Figure 16 and Figure 17 for YbAg and YbAu, respectively. These charts show the energy of the molecular orbitals of the diatomic molecules, with the colour of the bars determined by the size of the linear coefficient C_A. The active space cut-offs that were used when investigating the effect of freezing orbitals on W_d are indicated with horizontal dashed lines in both figures, along with the resulting W_d values.

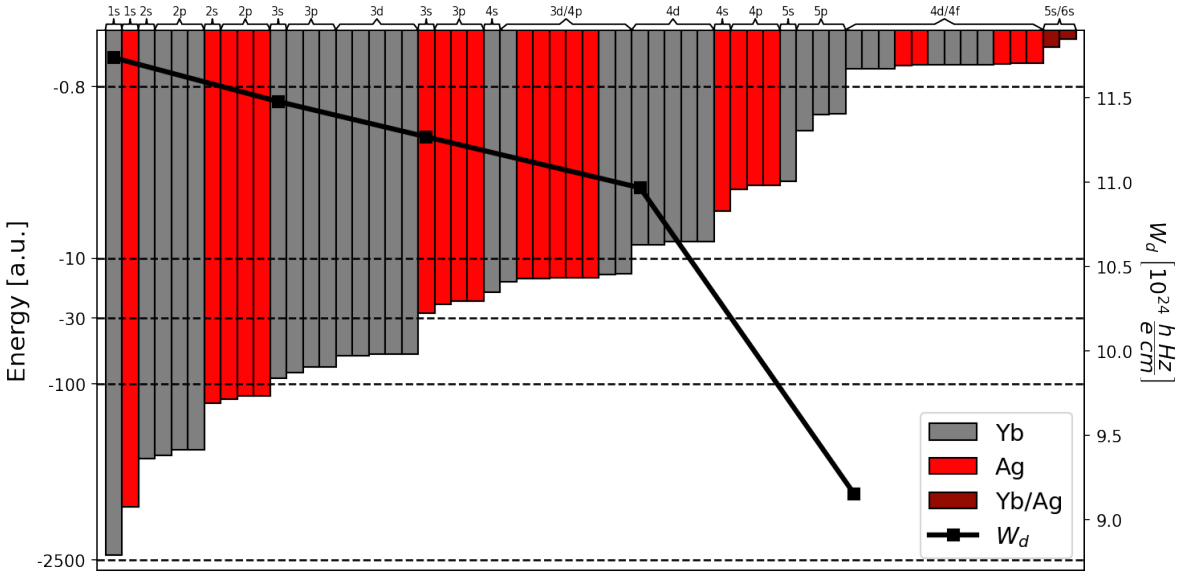

FIGURE 16. The energy of the molecular orbitals of YbAg. The used active space cut-offs are indicated with horizontal dashed lines.

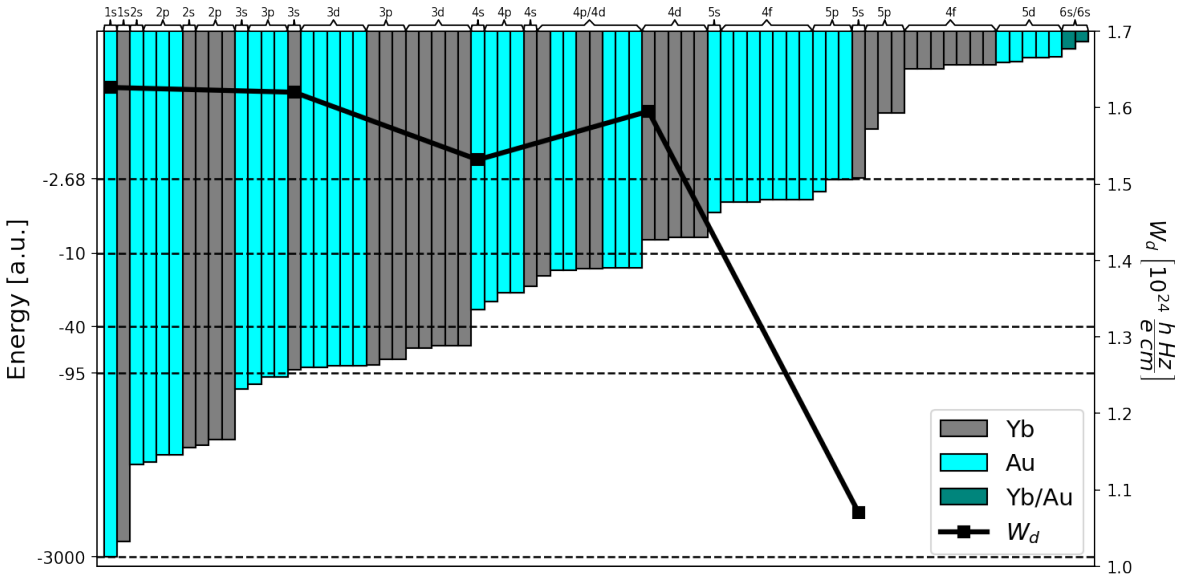

FIGURE 17. The energy of the molecular orbitals of YbAu. The used active space cut-offs are indicated with horizontal dashed lines.